SOLID STATE ELECTRONICS LABORATORY

STANFORD ELECTRONICS LABORATORIES
DEPARTMENT OF ELECTRICAL ENGINEERING
STANFORD UNIVERSITY · STANFORD, CA 94305

RAPID THERMAL PROCESSING OF III-V COMPOUND SEMICONDUCTORS WITH APPLICATION TO THE FABRICATION MICROWAVE DEVICES

FINAL REPORT

James F. Gibbons
Principal Investigator

May 1988

U.S. Army Research Office
Proposal Number 21616-EL
Contract DAAG29-85-K-0054
April 1, 1985 – March 31, 1988

UNCLASSIFIED
SECURITY CLASSIFICATION OF THIS PAGE

MASTER COPY - FOR REPRODUCTION PURPOSES

REPORT DOCUMENTATION PAGE

1a. REPORT SECURITY CLASSIFICATION: Unclassified	1b. RESTRICTIVE MARKINGS
2a. SECURITY CLASSIFICATION AUTHORITY	3. DISTRIBUTION / AVAILABILITY OF REPORT: Approved for public release; distribution unlimited.
2b. DECLASSIFICATION / DOWNGRADING SCHEDULE	
4. PERFORMING ORGANIZATION REPORT NUMBER(S)	5. MONITORING ORGANIZATION REPORT NUMBER(S): ARO 21616.8-EL
6a. NAME OF PERFORMING ORGANIZATION: Stanford University; 6b. OFFICE SYMBOL (If applicable)	7a. NAME OF MONITORING ORGANIZATION: U. S. Army Research Office
6c. ADDRESS (City, State, and ZIP Code): Stanford, CA 94305	7b. ADDRESS (City, State, and ZIP Code): P. O. Box 12211, Research Triangle Park, NC 27709-2211
8a. NAME OF FUNDING / SPONSORING ORGANIZATION: U. S. Army Research Office; 8b. OFFICE SYMBOL (If applicable)	9. PROCUREMENT INSTRUMENT IDENTIFICATION NUMBER: DAAG29-85-K-0054
8c. ADDRESS (City, State, and ZIP Code): P. O. Box 12211, Research Triangle Park, NC 27709-2211	10. SOURCE OF FUNDING NUMBERS: PROGRAM ELEMENT NO. / PROJECT NO. / TASK NO. / WORK UNIT ACCESSION NO.

11. TITLE (Include Security Classification)
Rapid Thermal Processing of III-V Compound Semiconductors with Application to the Fabrication of Microwave Devices

12. PERSONAL AUTHOR(S)
J. F. Gibbons

13a. TYPE OF REPORT	13b. TIME COVERED	14. DATE OF REPORT (Year, Month, Day)	15. PAGE COUNT
Final	FROM 4/1/85 TO 3/31/88	May 88	49

16. SUPPLEMENTARY NOTATION
The view, opinions and/or findings contained in this report are those of the author(s) and should not be construed as an official Department of the Army position, policy, or decision, unless so designated by other documentation.

17. COSATI CODES		
FIELD	GROUP	SUB-GROUP

18. SUBJECT TERMS (Continue on reverse if necessary and identify by block number)
Thermal Processing; Semiconductors, Compound Semiconductors, Surface Doping; Microwave Devices; Silicon Diffusion, Zinc Diffusion; Gallium Arsenide.

19. ABSTRACT (Continue on reverse if necessary and identify by block number)
This research was focused on establishing better techniques for surface doping of III-V semiconductors.

The GaAs doping techniques investigated in this work include Si surface duffusions using a solid source, ion implantation followed by rapid thermal annealing, and both solid source and vapor phase Zn diffusions. New models for Si duffusion/electrical activation, and Zn diffusion have been developed and implementated in computer simulations. Using these rapid thermal diffusion techniques, it was possible to demonstrate that shallow n^+ and p^+ layers can be produced reliably while retaining excellent surface morphology. In addition, an improved understanding of the annealing of defects and electrical activation of dopants in ion implanted, amorphized GaAs has been achieved.

20. DISTRIBUTION / AVAILABILITY OF ABSTRACT	21. ABSTRACT SECURITY CLASSIFICATION
☐ UNCLASSIFIED/UNLIMITED ☐ SAME AS RPT. ☐ DTIC USERS	Unclassified
22a. NAME OF RESPONSIBLE INDIVIDUAL	22b. TELEPHONE (Include Area Code) / 22c. OFFICE SYMBOL

DD FORM 1473, 84 MAR — 83 APR edition may be used until exhausted. All other editions are obsolete.

SECURITY CLASSIFICATION OF THIS PAGE
UNCLASSIFIED

RAPID THERMAL PROCESSING OF III-V COMPOUND SEMICONDUCTORS WITH APPLICATION TO THE FABRICATION OF MICROWAVE DEVICES

FINAL REPORT

J.F. Gibbons
Principal Investigator

May 1988

U.S. Army Research Office
Proposal Number 21616-EL
Contract DAAG29-85-K-0054
April 1, 1985 – March 31, 1988

Stanford University
Stanford, California 94305

FOREWORD

This document is the final report for U.S. Army Research Office contract number DAAG29-85-K-0054, which corresponds to the proposal entitled **Rapid Thermal Processing of III-V Compound Semiconductors With Application to the Fabrication of Microwave Devices**. This research is focused on establishing better techniques for surface doping of III-V semiconductors. Portions of this work were carried out in conjunction with our research on Limited Reaction Processing and MOCVD of compound semiconductors, under a previous ARO contract, DAAG29-85-K-0237.

The GaAs doping techniques investigated in this work include Si surface diffusions using a solid source, ion implantation followed by Rapid Thermal Annealing, and both solid source and vapor phase Zn diffusions. New models for Si diffusion/electrical activation, and Zn diffusion have been developed and implemented in computer simulations. Using these rapid thermal diffusion techniques, we have demonstrated that shallow n^+ and p^+ layers can be produced reliably while retaining excellent surface morphology. In addition, an improved understanding of the annealing of defects and electrical activation of dopants in ion implanted, amorphized GaAs has been achieved.

This report constitutes a brief summary of research performed under the above contract. It begins in Part 1 with a list of publications associated with this research. A short synopsis of 7 publications which describe our findings is followed by Part 3, which contains reprints of these publications. The final section (Part 4) contains a list of participating scientific personnel.

CONTENTS

Part 1

List of Publications

The following is a list of 7 publications which are summarized in Part 2 of this report. Reprints of these articles appear in Part 3 in the following order:

1. Mark E. Greiner and James F. Gibbons, "Diffusion and electrical properties of silicon-doped gallium arsenide", *J. Appl. Phys.* **57**, 15 June 1985, pp. 5181-5187.

2. W.G. Opyd and J.F. Gibbons, "Regrowth of amorphized compound semiconductors", *Mat. Res. Soc. Symp. Proc. Vol.* **45**, (Materials Research Society, Pittsburg, 1985), pp. 273-277.

3. W.G. Opyd, J.F. Gibbons, J.C. Bravman, and M.A. Parker, "Damage calculation and measurement for GaAs amorphized by Si implantation", *Appl. Phys. Lett.* **49**, 13 October 1986, pp. 974-976.

4. W.G. Opyd, J.F. Gibbons, and A.J. Mardinly, "Precipitation of Impurities in GaAs Amorphized by Ion Implantation", submitted to *Appl. Phys. Lett.*, May 1988.

5. S. Reynolds, D.W. Vook, and J.F. Gibbons, "Limited reaction processing: Growth of III-V epitaxial layers by rapid thermal metalogranic chemical vapor deposition", *Appl. Phys. Lett.* **49**, 22 Dec. 1986, pp. 1720-1722.

6. S. Reynolds, D.W. Vook, W.G. Opyd, and J.F. Gibbons, "Rapid thermal annealing of Si-implanted GaAs with trimethylarsenic overpressure", *Appl. Phys. Lett.* **51**, 21 Dec. 1987, pp. 916-918.

7. S. Reynolds, D.W. Vook, and J.F. Gibbons,"Open-tube Zn diffusion in GaAs using diethylzinc and trimethylarsenic: Experiment and model", *J. Appl. Phys.* **63**, 15 Feb. 1988, pp. 1052-1059.

Part 2

Summary of the Research

Rapid Thermal Processing (RTP) offers several important advantages over furnace annealing of GaAs. In fact, because of difficulties associated with surface decomposition, the arguments in favor of employing RTP are often more compelling for compound semiconductors than for silicon. For a bare surface, arsenic and gallium loss rates are very high (10^{16} /cm^2 – sec. at 800 °C) at temperatures required to anneal implant damage or perform dopant diffusion in GaAs. Hence, limiting the time at temperature is important for GaAs processing. In addition, because of the system design, it is usually easier to control the ambient during RTP compared to furnace processing. Using RTP, we have also been able to study fundamental processes such as diffusion and implant damage annealing in a time/temperature regime not accessible with conventional techniques.

2.1 Si Diffusion in GaAs

Applications of thin, heavily Si-doped layers include source and drain contacts for GaAs MESFETS . Work performed as part of a previous ARO contract included a study of RTP employed to diffuse Si into GaAs from a thin elemental source. Si_3N_4 and SiO_2 encapsulants were used in these experiments. Diffusions were performed at temperatures as high as 1050 °C for times as short as 3 sec. Si was observed to diffuse into GaAs at depths up to 0.3 μm for SiO_2 capped samples. Under otherwise identical conditions, no diffusion was detected for Si_3N_4 encapsulated GaAs.

In the early part of the present contract period, we developed a complete diffusion model for Si in GaAs to explain the measured RTA data. This model is described in Paper # 1 in Section 3. The Si diffusion mechanism is based upon the formation of nearest-neighbor donor-acceptor pairs. The diffusion front is very steep due to pair dissociation at low dopant concentrations. Several experiments

which support the application of this mechanism to high concentration Si diffusion in GaAs are discussed. A compensation mechanism for amphoteric dopants is developed as well. These models are potentially applicable to all amphoteric dopants in III-V compounds where dopant pairing is likely to dominate the diffusion process.

2.2 Solid phase epitaxy of compound semiconductors

Paper # 2 describes the initial motivations for an investigation of solid phase epitaxy (SPE) in compound semiconductors, which include the possibility of lower temperature anneals, as in the case of silicon, which would result in reduced material decomposition and impurity diffusion. The thresholds for amorphization of InSb and GaAs are reported based upon correlations of Boltzmann transport calculations with experimental observations.

Paper # 3 presents a study of the stages of defect annealing following the SPE of an amorphous layer. Material is analyzed over a range of annealing temperatures by transmission electron microscopy (TEM) and Rutherford backscattering spectrometry. Though SPE occurs at low temperatures, residual defect annealing is noted to require higher temperatures.

Paper # 4 describes an investigation of the problem of failure to achieve electrical activation of implanted impurities even after high temperature defect anneals. Photoluminescence, TEM, and x-ray microanalysis are used to show that the lack of electrical activation is associated with the precipitation of stable, electrically neutral impurity complexes. This result is shown to be similar to that observed for low temperature MBE and demonstrates a technique for precipitating impurities in GaAs.

As part of a companion contract, we have developed a III-V, Rapid Thermal MOCVD system, as described in Paper # 5. Besides epitaxial growth, we were also able to use this system to study Rapid Thermal Annealing of Si implants in GaAs in a trimethylarsenic overpressure. As described in Paper # 6, we have compared Si implant activation efficienty and surface degredation for arsenic ambient and proximity capped anneals. The arsenic ambient gives consistenly higher implant activation with better surface morphology.

2.3 Zn Diffusion in GaAs

Zn diffusion in GaAs is an important processing step in the fabrication of diodes, junction field-effect transistors, and bipolar transistors. Using conventional sealed ampoule methods, control over the diffusion process is often difficult, and poor surface morphology and variable junction depths can limit device performance. Using the organometallic sources diethylzinc (DEZn) and trimethylarsenic (TMAs), we have characterized the diffusion of Zn into GaAs, as described in Paper # 7. This method produces surface hole concentrations in excess of 10^{20} cm^{-3}, with good control of junction depths as shallow as 0.1 μm. A key advantage of this method is the smooth surface morphologies obtained.

As discussed in Paper # 7, diffusions were carried out in a hot-wall quartz reaction chamber at atmospheric pressure. The gas delivery system is essentially the same one which is described in Papers 5 and 6. Using our MOCVD reactor to perform vapor phase diffusions allows us to accurately meter the quantities of reactants delivered to the wafer. We were able to independently control the time, temperature, and partial pressures of As and Zn, as well as the total pressure, which can not be done using the conventional ampoule method. In total, over 40 diffusion samples were analyzed by SIMS and Hall effect measurements.

Paper # 7 describes the results in detail. These diffusions have a complex double profile which is not predicted by the widely accepted interstitial-substitutional model for Zn diffusion. We suggest that this double profile may be caused by the existence of two mobile Zn species which dominate in different regions according to the position of the local Fermi level. We have implemented a computer simulation which gives an approximate solution based upon this model, and provides a good fit to both our data, and that of several other authors. Our model shows that a double diffusion profile does not necessarily imply vacancy (or interstitial) nonequilibrium.

Part 3

Reprints of Publications

This sections contains reprints of the articles listed in Part 1 and described in Part 2.

Diffusion and electrical properties of silicon-doped gallium arsenide

Mark E. Greiner[a] and James F. Gibbons
Stanford Electronics Laboratory, Stanford University, Stanford, California 94305

(Received 9 October 1984; accepted for publication 4 January 1985)

The amphoteric nature of silicon in gallium arsenide is used to develop diffusion and electrical compensation mechanisms. The diffusion mechanism is based on the formation and diffusion of nearest-neighbor donor-acceptor pairs. General solutions are presented that predict abrupt diffusion fronts for a wide range of pairing conditions. Experiments support the application of this mechanism to Si diffusion in GaAs at high concentrations. A compensation mechanism for amphoteric dopants is developed as well. The compensation process is driven primarily by the free-electron concentration. Nearly complete compensation is predicted for large dopant concentrations.

I. INTRODUCTION

Except for a few attempts,[1-3] Si diffusion has not been used to form *n*-type layers in GaAs. Because of this, a well-developed technology for Si diffusion does not exist at this time. The current processes for forming *n*-type layers in GaAs involve the growth of epitaxial layers and the implantation of *n*-type dopants into semi-insulating GaAs. In the latte case, studies were done[4-7] on the Si diffusion which occurs during subsequent annealing of these ion-implanted layers. The concentrations of implanted Si in these studies are limited to those used in GaAs field effect transistor channels and are generally in the $10^{17}/cm^3$ range. This study focuses on Si in GaAs diffused from the surface under conditions that result in heavily doped *n*-type layers. A diffusion model and a compensation model are developed for amphoteric dopants and applied to Si doping in GaAs.

Before presenting the results from this work, two sets of published diffusion data will be reviewed. The first set contains the early diffusion work by Vieland[1] and Antell,[2] who use Si vapor and solid sources, respectively, to form diffused layers, and recent work by the present authors.[3] The second set of data to be reviewed deals with diffusion of low-dose, ion-implanted Si. These results will be useful as a comparison to the diffusion effects observed at high concentrations.

II. REVIEW OF Si DIFFUSION

A. High Si concentrations

Both Vieland and Antell reported the effect of arsenic pressures on diffusion rates in GaAs. Vieland diffused Si into GaAs at 1150 °C and relied on the vapor pressure of Si over a solid Si source ($\sim 10^{-6}$ Torr) to provide the dopant. In Antell's work, Si was diffused from a 3000-Å Si film sputtered directly onto a *p*-type GaAs sample. All anneals took place in evacuated ampoules containing solid arsenic to produce the desired arsenic overpressures. For all three temperatures studied, the junction depth increased rapidly with increasing arsenic overpressure until a knee was reached at some pressure P_K. Above this pressure, the junction depth became independent of pressure. Without a detailed knowledge of the GaAsSi ternary diagram, it is difficult to interpret this knee.

The arsenic overpressure is predicted to vary the concentration of gallium and arsenic vacancies by the interaction between the arsenic vapor and the GaAs surface. The magnitude of these variations is expressed in the following equations[1]:

$$[V_{Ga}] = k_1 \cdot P_{As_4}^{1/4} \tag{1}$$

and

$$[V_{As}] = k_2 \cdot P_{As_4}^{-1/4}. \tag{2}$$

By comparing this vacancy dependence on As overpressure with the experiments of Vieland and Antell above, we see that the diffusion rate of Si increases with the surface concentration of gallium vacancies.

In addition to the junction depth, Antell measured a free-carrier concentration of $5 \times 10^{18}/cm^3$ for a 1000 °C diffusion. This concentration was constant throughout the diffused layer. The surface concentration was estimated to be greater than $10^{20}/cm^3$ showing a high level of electrical compensation in these diffused layers.

In a recent study by the present authors[3] rapid thermal processing was used to diffuse Si into GaAs from a thin elemental source. The sample structure is shown in Fig. 1. Si_3N_4 and SiO_2 encapsulants were used here rather than As overpressures. Diffusions were performed at temperatures as high as 1050 °C for times as short as 3 sec. Si diffusion into GaAs up to 0.3 μm was observed for SiO_2 encapsulated samples. No diffusion was detected for Si_3N_4 encapsulated samples for the short time used in this process.

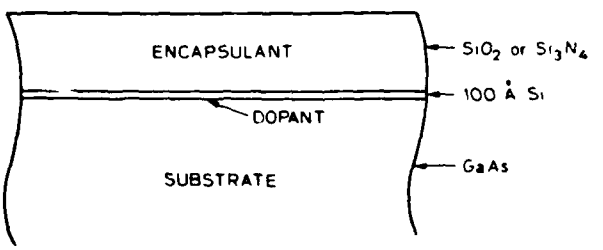

FIG. 1. Sample structure used to diffuse Si into GaAs during rapid thermal processing.

[a] Current address: Cincinnati Electronics Corporation, 2630 Glendale-Milford Road, Cincinnati, Ohio 45241.

 0021-8979/85/125181-07$02.40

Secondary ion mass spectroscopy (SIMS) was used to measure the Si diffusion profiles. The resulting profiles indicated a concentration-dependent diffusion coefficient. The Si diffusion front was very steep, similar to the diffusion profiles produced by zinc diffusion in GaAs. Although both Zn and Si exhibit these abrupt diffusion fronts, they behave differently under As overpressures. Zn is believed to diffuse by an interstitial-substitutional mechanism.[8] Increasing the As overpressure retards the Zn diffusion process,[9] in agreement with the interstitial-substitutional mechanism. In contrast, Si diffusion is enhanced under As overpressures.[1,2] Also, the activation energy for the Si diffusion process at high concentrations was measured to be 2.5 eV,[3] which is in the range associated with substitutional diffusion in GaAs.

A substitutional mechanism was proposed[3] for Si diffusion in GaAs based upon the formation and diffusion of Si nearest-neighbor pairs. This model assumes that Si pairs dominate the diffusion flux at high Si concentrations. Since the pair concentration is a function of the total Si concentration, a concentration-dependent diffusion coefficient is predicted by this mechanism. This model provides a good fit to the profiles produced by Si diffusion during rapid thermal processing.

B. Low Si concentrations

There have been many reports on the electrical profiles produced by implanting Si^+ into semi-insulating GaAs.[4-7] After the implant, the silicon is made electrically active by a postimplant anneal. These anneals use some method designed to eliminate surface erosion due to preferential As evaporation. The resulting electrical profiles depend on the method used during the postimplantation anneal. As a result, reported diffusion coefficients vary over a wide range. The results from several authors are summarized in Table I.

No two sets of experiments were found with identical implant and annealing conditions. The results in Table I cover the range of techniques commonly used in furnace annealing. In all cases when diffusion was measurable, the as-implanted profiles were simply broadened while maintaining their as-implanted shape. The retention of the as-implanted shape under all annealing conditions implies there is a common diffusion mechanism in which the diffusion coefficient of Si is not a function of concentration over the range of concentrations studied. These concentrations are less than $10^{18}/cm^3$. However, concentration-dependent diffusion was observed at Si concentrations between $10^{18}/cm^3$ and $10^{20}/cm^3$.[3]

The value of the diffusion coefficient for these low Si concentrations depends upon the specific annealing conditions. In a study by Kasahara and Watanabe,[6] the diffusion of low-dose Si^+ implants in unencapsulated GaAs was measured after annealing at 900 °C under various partial pressures of AsH_3. The diffusion rate was found to increase with the fourth root of the AsH_3 partial pressure for pressures greater than 0.2 Torr. Two of these values are listed in Table I. This dependence is similar to that obtained by Vieland and Antell for high-concentration diffusion under As overpressures.

The diffusion data for Onuma *et al.*[7] in Table I for encapsulated anneals show a dependence on the type of encapsulant. SiO_2 encapsulated anneals produced Si diffusion rates 20 times greater than anneals using Si_3N_4 encapsulation. It was suggested[7] that this enhanced diffusion under SiO_2 encapsulation was related to the excessive out-diffusion of Ga from the GaAs into the SiO_2.[10] This Ga loss was believed to produce excess Ga vacancies at the GaAs surface. Thus, enhanced diffusion of Si under SiO_2 encapsulation is similar to the enhanced diffusion under As[1,2] and AsH_3[6] overpressures in that both techniques produce excess Ga vacancies.

In another study, Kasahara *et al.*[5] showed that the thickness of the encapsulant affects the diffusion rate of Si in GaAs. The diffusion rate at 850 °C under Si_3N_4 encapsulation increased by 20% when the encapsulant thickness was increased from 500 to 1000 Å. Since the interfacial stress produced by an encapsulant scales directly with its thickness, this thickness dependence suggested a stress-enhanced diffusion rate.

In a similar study by Onuma *et al.*[7] of Si diffusion under Si_3N_4 encapsulation, the measured diffusion rate was only 8% of the value measured by Kasahara *et al.*[5] although the experimental conditions were nearly identical. Both of these measurements were made after 850 °C anneals using a 0.1-μm Si_3N_4 encapsulant deposited by chemical vapor deposition techniques. Since the stress in Si_3N_4 films is known to depend on the deposition parameters,[11] Si diffusion rates enhanced by stress should show some dependence on Si_3N_4 deposition conditions. Different encapsulant stresses could explain the discrepancy between the results of these two experiments.

In addition to the possibly different Si_3N_4 deposition parameters, the samples were annealed in different atmospheres. Kasahara *et al.* measured the faster Si diffusion for

TABLE I. Summary of diffusion constants for Si in GaAs extracted from electrical measurements for a wide range of postimplantation annealing conditions.

Author	Reference	Anneal ambient	Encapsulant	Anneal temperature	Diffusion constant
Lee *et al.*	4	H_2 over GaAs/Ga	None	800 °C	Nondetectable
Kasahara *et al.*	5	5-Torr AsH_3 in H_2	None	850 °C	8×10^{-13} cm²/sec
Kasahara *et al.*	5	5-Torr AsH_3 in H_2	0.1-μm Si_3N_4	850 °C	1.2×10^{-14} cm²/sec
Onuma *et al.*	7	H_2	0.12-μm Si_3N_4	850 °C	1×10^{-13} cm²/sec
Onuma *et al.*	7	H_2	0.2-μm SiO_2	850 °C	2×10^{-12} cm²/sec
Kasahara *et al.*	6	5-Torr AsH_3 in H_2	None	900 °C	2×10^{-12} cm²/sec
Kasahara *et al.*	6	0.3-Torr AsH_3 in H_2	None	900 °C	1×10^{-13} cm²/sec

samples annealed in 5-mTorr AsH_3 in H_2 while Onuma's samples were annealed in 100% H_2. Previous results by Kasahara and Watanabe[6] showed that the Si diffusion rate in unencapsulated GaAs increased with AsH_3 partial pressure. Although the present discrepancy involves Si_3N_4 encapsulated samples, some communication between the AsH_3 and GaAs may have occurred through the encapsulant.

In summary, for all the cases reviewed here where the concentration of Si is low, the diffusion process can be modeled using a constant diffusion coefficient. It is clear from these experiments, however, that the value of the Si diffusion constant in GaAs depends on the condition of the GaAs surface. Encapsulants and arsenic-bearing overpressures can vary the diffusion rates over an order of magnitude. These annealing conditions increase the concentration of Ga vacancies, suggesting that Ga vacancies are an important part of the Si diffusion process.

Results from Si diffusion experiments at high Si concentrations exhibited a similar dependence on encapsulation and arsenic overpressures. However, the basic diffusion process appears to be different and can be modeled with a Si pair mechanism. In the next section, this pair diffusion mechanism will be developed fully, and solutions to the diffusion equation will be presented that cover a range of pairing conditions.

III. A MODEL FOR DIFFUSION OF AMPHOTERIC DOPANTS IN III-V SEMICONDUCTORS

A. Assumptions

Recently, it was observed that Si diffusion into GaAs could be modeled by a Si pair diffusion mechanism when Si was present in large concentrations.[3] Here, we generalize this pair mechanism to any amphoteric dopant in a III-V semiconductor by solving the diffusion equation under a wide range of pairing conditions.

A column IV dopant forms a donor when occupying a column III lattice site and forms an acceptor when occupying a column V lattice site. Two column IV dopants residing on nearest-neighbor donor-acceptor sites form a neutral pair. It is this neutral pair which is assumed to be the mobile diffusion species. The concentrations of these dopant configurations are written as C_d, C_a, and C_p, respectively. The total concentration of the column IV dopant becomes

$$C_T = C_d + C_a + 2C_p. \tag{3}$$

Before proceeding with a diffusion model involving these neutral pairs, their concentration must by quantified. To calculate the percent of the dopant existing as pairs we need to make the following assumptions. First, neutral pairs are assumed to be in equilibrium with donors and acceptors. This is written for Si-doped GaAs as

$$Si_{Ga}^{+} + Si_{As}^{-} \rightleftarrows Si_{Ga} - Si_{As}. \tag{4}$$

The law of mass action can be applied to this reaction to relate the relative concentrations of donors, acceptors, and pairs. This results in the following pair equilibrium equation:

$$C_d \cdot C_a = K_p \cdot C_p, \tag{5}$$

where K_p is the pair equilibrium constant.

Second, if the dopant concentration is high such that the semiconductor is heavily compensated, we can set the donor and acceptor concentrations essentialy equal. This is written as

$$C_d = C_a. \tag{6}$$

This second assumption fails at low doping levels where most amphoteric dopants preferentially form either donors or acceptors. The doping concentration where this occurs depends upon the specific dopant and the host lattice as well as temperature and annealing conditions.

Using Eqs. (3), (5), and (6) we solve for the fraction of the dopant that is paired, $2C_p/C_T$, in terms of the total dopant concentration. The result is

$$\frac{2C_p}{C_T} = 1 + \frac{K_p}{C_T}\left(1 - \sqrt{1 + 2C_T/K_p}\right). \tag{7}$$

The percent of the dopant paired is plotted in Fig. 2 versus total dopant concentration C_T normalized to the pair equilibrium constant K_p. For $C_T/K_p = 1$, 27% of the dopant is predicted to be paired with the percent paired increasing with total concentration.

We now wish to solve the diffusion equation assuming that dopant pairs dominate the diffusion process. Under these conditions, the dopant flux can be written (in one dimension) as

$$\text{Flux} = -2 \cdot D_p \cdot \frac{\partial C_p}{\partial x}, \tag{8}$$

where D_p is the pair diffusion constant. Since the concentration of pairs can be expressed in terms of the total dopant concentration using Eq. (7), we can rewrite the flux equation in a more convenient form as

$$\text{Flux} = -D_{\text{eff}} \cdot \frac{\partial C_T}{\partial x}, \tag{9}$$

where

$$D_{\text{eff}} = 2 \cdot D_p \cdot \frac{\partial C_p}{\partial C_T}. \tag{10}$$

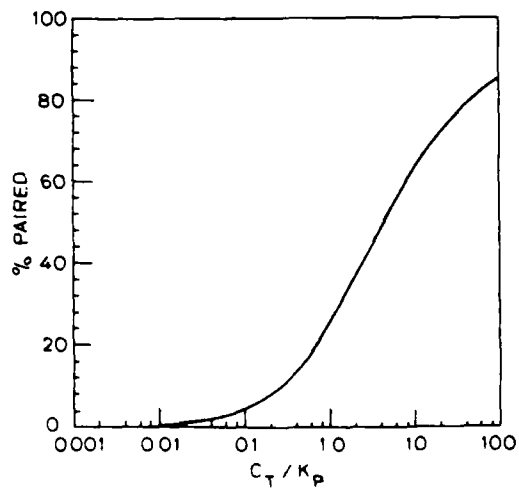

FIG. 2. Percent of an amphoteric dopant existing as pairs as a function of the total dopant concentration normalized to the pair equilibrium constant.

Using Eq. (7) to evaluate the derivative in Eq. (10) we have

$$D_{eff} = D_p\left[1 - (1 + 2C_T/K_p)^{-1/2}\right]. \quad (11)$$

This effective diffusion coefficient resulting from pair diffusion is dependent upon the dopant concentration. For large concentrations ($C_T \gg K_p$), the second term in the brackets in Eq. (11) drops out. The effective diffusion coefficient then becomes constant and equal to D_p. As the total dopant concentration drops, the effective diffusion coefficient decreases due to a pair concentration which is dropping faster than the total dopant concentration.

B. Solution to the diffusion equation

The diffusion equation can be solved using the effective diffusion coefficient in Eq. (11) and assuming a constant surface concentration C_0. Since the value of the pair equilibrium constant can vary over a wide range depending on the specific dopant, solutions will be presented for several values of K_p. The presentation of the solutions can be simplified by noting that the Boltzmann substitution, $\eta = x/2\sqrt{t}$, can be applied to this diffusion model. Thus, the depth scale is normalized to $\sqrt{D_p t}$, where D_p is the pair diffusion coefficient and t is the diffusion time. The concentration scale is normalized to the surface concentration C_0. The solution of the diffusion equation for several pair equilibrium constants is shown in Fig. 3 with these normalized coordinates.

For low values of K_p, a deeper diffusion is observed. This is due to the greater pairing which is predicted for these low values of K_p. To emphasize this point, we note that for $C_T = 0.1C_0$, 8% pairing is predicted for $K_p = 0.5C_0$ while 38% pairing is predicted for $K_p = 0.05C_0$. Thus, for the same pair diffusion constant and diffusion time, a deeper diffusion is produced by the lower pair equilibrium constants.

For all values of K_p, Fig. 3 shows very steep diffusion fronts. This effect can be understood if the diffusion process is visualized in the following steps. Some of the dopant enters the lattice as neutral pairs. These pairs are highly mobile and quickly move to the diffusion front where the total dopant concentration is low. Here the pairs dissociate into less mobile single donors and acceptors as predicted by Eq. (5). Diffusion beyond this region then proceeds very slowly due to the low concentration of dopant pairs. The result is a very steep diffusion front. Deeper diffusions produced by a higher pairing percentage do not begin the disassociation process until much lower concentrations.

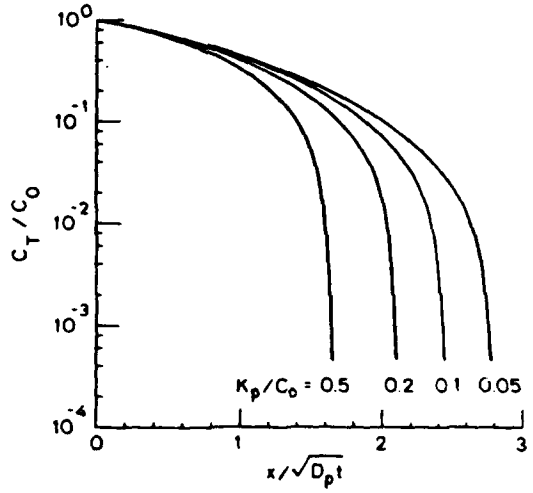

FIG. 3. Solutions to the diffusion equation assuming a pair diffusion mechanism and a constant surface concentration for various pairing conditions.

At this time, two limitations of this model should be mentioned. First, the flux of single diffusing species may become important at low concentrations where the concentration of dopant pairs becomes negligible. This model will not predict accurately the diffusion at low concentrations since mechanisms not included in the model may become significant. Second, the calculation of the pair concentration is not accurate for dopant concentrations near the measured electron concentration. Here, the assumption of complete compensation breaks down, and the donor and acceptor concentrations are no longer equal. The results of the model are not affected significantly since correction of this second approximation decreases the calculated pair concentration which increases the slope of the steep diffusion front.

In summary, a diffusion model involving the formation and rapid diffusion of neutral dopant pairs predicts concentration-dependent diffusion profiles. The diffusion front is very steep due to the pair dissociation at low dopant concentrations. The junction depth is dependent on the pair diffusion constant, diffusion time, and pair equilibrium constant. This model is potentially applicable to all amphoteric dopants in III-V compounds where dopant pairing is likely to dominate the diffusion process.

IV. Si DIFFUSION IN GaAs

A. Si pair equilibrium constant

The pair diffusion mechanism presented in the last section predicts diffusion profiles that can be shown to agree with Si diffusion profiles in GaAs at high concentrations.[3] Here, a pair equilibrium constant of $4\times10^{19}/cm^3$ provides the best fit for Si diffusion at 1050 °C. This gives a normalized pair equilibrium constant of $K_p/C_0 = 0.2$ for the measured Si surface concentration of $2\times10^{20}/cm^3$. A sample of this fit is shown in Fig. 4.

The application of this pair mechanism to Si diffusion in GaAs would be supported strongly by an independent measurement of the Si pair equilibrium constant. An estimate of this constant can be obtained from measurements of the infrared absorption in Si-doped GaAs due to localized vibrational modes. In a study by Kung and Spitzer,[12] absorption due to Si donors, acceptors, and pairs was measured in GaAs samples uniformly doped with 4×10^{19} Si/cm^3. If one assumes all Si atoms to have the same absorption cross section, the concentrations of Si donors, acceptors, and pairs can be calculated from the area of these absorption peaks and the total Si concentration. These values are found in Ref. 12 for three separate samples annealed at 1100 °C and are listed in Table II. The pair association constant for 1100 °C can be

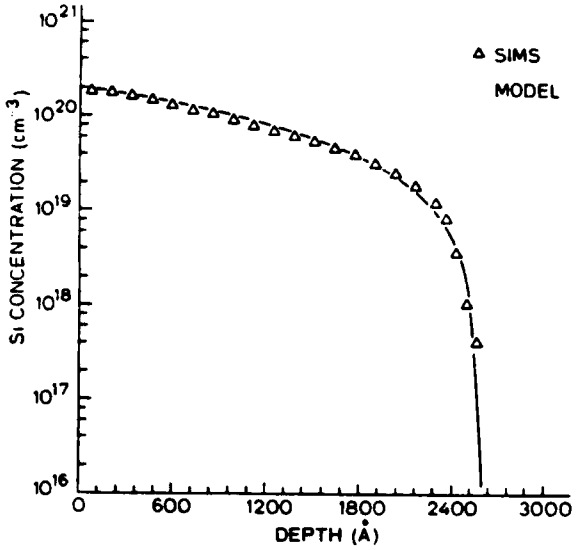

FIG. 4. SIMS profile for a 1050 °C Si diffusion into GaAs with a calculated pair diffusion profile using $D_p t = 1.5 \times 10^{-10}$ cm^2 and $K_p/C_0 = 0.2$.

calculated using these values in Eq. (5) and is also listed in Table II for each sample. These values are very close to the value of K_p which gave the best fit to the Si diffusion profile of Ref. 3. The fact that this independent measurement of the pair equilibrium constant agrees with the value used to fit the pair diffusion mechanism to Si diffusion data strongly supports the application of this model to Si diffusion in GaAs.

B. Atomic jump process of Si pairs

Mechanisms for Si diffusion that involve motion of isolated silicon atoms through Ga and As vacancies require changes in vacancy type and charge state that would presumably produce very low diffusion coefficients. However, the diffusion of a nearest-neighbor dopant pair is much simpler. Paired Si atoms can move substitutionally by exchanging sites with either a Ga or As vacancy. The leading Si atoms moves into an adjacent vacancy with the trailing Si atom leaving behind the original vacancy. This process is expressed by the following equation:

$$Si_{Ga} - Si_{As} + V_{Ga} \rightarrow V_{Ga} + Si_{As} - Si_{Ga},$$

with a similar expression for a pair exchange with an As vacancy.

Si pairs move through the GaAs lattice by alternating exchanges with Ga and As vacancies. The rate at which these exchanges occur will depend upon the number of Si pairs which have the energy required for the exchange and on the fraction of the time that an adjacent lattice site is vacant. The first effect is temperature dependent, and the second is proportional to the Ga and As vacancy concentrations. Calculations[13] and experiment[14] have suggested that the arsenic vacancy concentration exceeds the gallium vacancy concentration by at least one order of magnitude. Because of the lower Ga vacancy concentration, one would expect the waiting time for Ga vacancies to be much longer than for As vacancies. This would make the Si pair–Ga vacancy exchange the rate-limiting step in the diffusion process. Any moderate change in the concentration of As vacancies should not affect the diffusion rate while an increase in the Ga vacancy concentration should result in a corresponding increase in the overall diffusion rate.

In an experiment by Vieland[1] described in Sec. II, an increase in the arsenic overpressure during diffusion of heavily Si-doped GaAs produced an increase in the Si diffusion rate. As overpressures are believed to increase the concentration of Ga vacancies. Thus, this result is in agreement with the suggestion above that Si pair exchange with a Ga vacancy is the rate-limiting step in the pair diffusion mechanism. For Si diffusion into GaAs during rapid thermal processing, SiO_2 encapsulation greatly enhanced the diffusion rate. Since Ga dissolution by SiO_2 is believed to produce excess Ga vacancies, this enhancement also suggests that the Si pair–Ga vacancy exchange is the rate-limiting step in the Si diffusion process. Thus, vacancies are an important consideration in the diffusion process. In the next section, we consider the effect of vacancies on the electrical properties of Si-doped GaAs as well.

V. ELECTRON COMPENSATION EFFECTS IN Si-DOPED GaAs

A. Review

Diffusion of Si into GaAs from a thin-film source introduced Si at levels well above the measured electron concentration.[2,3] For diffusions at 1050 °C, the electron concentration was uniform throughout the diffused region at 5.5×10^{18}/cm^3 while the Si concentration was as high as 2×10^{20}/cm^3 at the surface. This saturation effect is present in other doping processes as well. Davies *et al.*[15] reported a maximum electron concentration of 6.5×10^{18}/cm^3 for an-

TABLE II. Relative infrared absorption in Si-doped GaAs due to various Si configurations for three samples annealed at 1100 °C. Also listed are the pair equilibrium constants calculated with Eq. (5).

Sample	Relative absorption			Pair equilibrium constant K_p
	Si_{Ga}	Si_{As}	Si_{Ga}-Si_{As}	
4	212	96	45	4.5×10^{19}/cm^3
5	211	82	45	4.0×10^{19}/cm^3
6	225	91	42	4.9×10^{19}/cm^3

nealed Si implants where the peak Si concentration was $2\times10^{19}/cm^3$. Chai *et al.*[16] showed that electron concentrations in Si-doped molecular beam epitaxy GaAs peak at $6\times10^{18}/cm^3$ while a group from Rockwell[17] obtained a higher activation by changing the growth conditions.

These electron saturation effects have been explained by a number of methods. There are electronic degeneracy effects in semiconductors that predict some form of free-carrier saturation at high doping levels. Effects due to the chemical solubility of impurities also have been used to explain free-carrier saturation effects in GaAs. In Te-doped GaAs, the formation of a stable precipitate, Ga_2Te_3, is believed to prevent the incorporation of single substitutional Te above levels of $10^{19}/cm^3$.[18] For doping by Si, Ge, and Sn, free-electron saturation can be attributed to dopant precipitation. However, since these dopants are amphoteric, the formation of compensating acceptors and neutral donor-acceptor pairs can produce the free-electron saturation observed under heavy doping conditions. Here, we propose a mechanism that predicts the formation of compensating acceptors and pairs at high electron concentrations which may be a significant part of the electron saturation effect found in heavily Si-doped GaAs. The mechanism is applicable to other amphoteric dopants in III-V compounds as well.

B. Compensation mechanism and predicted saturation profiles

The equilibrium between single Si and vacancies can be expressed by the following reaction:

$$Si_{Ga}^{+} + V_{As}^{+} + 2e^{-} \rightleftarrows Si_{As}^{-} + V_{Ga}^{-} + 2h^{+} \qquad (12)$$

Based on this compensation reaction, the site location of Si in GaAs will be affected by the electron and hole concentrations as well as As and Ga vacancy concentrations. To model the compensation in Eq. (12), all donors (Si_{Ga} and V_{As}) and acceptors (Si_{As} and V_{Ga}) are treated as completely ionized. In view of the Fermi-level position and the temperatures used in this study, this is a good assumption for all species except V_{As} which does not have a well-characterized donor level. Whether the As vacancies are neutral or ionized will not change the basic results of the compensation mechanism.

If equilibrium exists among the species in Eq. (12), the law of mass action can be used to calculate their relative concentrations. The result is

$$[Si_{Ga}^{+}]\cdot[V_{As}^{+}]\cdot n^2 = K_c\cdot[Si_{As}^{-}]\cdot[V_{Ga}^{-}]\cdot p^2, \qquad (13)$$

where the brackets [ ] denote concentration. The equilibrium constant K_c is related to the activation energy for the reaction in Eq. (12). Free-carrier saturation is inherent in this mechanism and can be seen by observing the effect of changing n or p on the distribution of Si between Ga and As sites. We assume for now that the vacancy concentrations are fixed. By increasing n in Eq. (13), Si shifts from Ga sites to As sites to maintain equilibrium. This reduces the donor concentration and increases the acceptor concentration, decreasing n. The reverse effect occurs when p is increased in Eq. (13).

The sensitivity of the compensation to the electron concentration can be extracted from Eq. (13) by solving for the Si acceptor to donor ratio γ. This is also called the compensation ratio and is shown below:

$$\gamma = \frac{[Si_{As}^{-}]}{[Si_{Ga}^{+}]} = \frac{1}{K_c(T)}\cdot\frac{[V_{As}^{+}]}{[V_{Ga}^{-}]}\cdot\left(\frac{n}{n_i}\right)^4. \qquad (14)$$

Thus, the compensation ratio is predicted to be proportional to the fourth power of the electron concentration. These results are based on positively charged As vacancies. The compensation ratio will be proportional to the third power of the electron concentration if the As vacancies are neutral.

In some liquid phase epitaxy layers, Si doping produces p-type conductivity. Under these conditions $[Si_{As}^{-}] > [Si_{Ga}^{+}]$ and $\gamma > 1$. Growth occurs under Ga melts which produce larger As to Ga vacancy concentration ratios than other epitaxial processes. According to Eq. (13), these conditions increase the compensation ratio. This p-type conductivity for Si doping is rare, however. For most epitaxial growth and annealing conditions using low Si concentrations, only Si donors are produced resulting in nearly uncompensated n-type conduction. For these conditions, $\gamma \ll 1$. For larger Si concentrations, conduction is still n type but with higher compensation.

From Eq. (13), the compensation ratio is predicted to increase with the fourth power of the electron concentration to the intrinsic concentration ratio, $(n/n_i)^4$. For Si concentrations and anneal temperatures where the electronic conduction is intrinsic ($n = n_i$), the compensation ratio γ is predicted to be independent of donor and acceptor concentrations. Under these intrinsic conditions, the Si and donor concentrations are usually found to be equal, implying $\gamma \ll 1$. However, as the doping increases and semiconductor becomes extrinsic ($n > n_i$), the compensation ratio is predicted to be increased by the $(n/n_i)^4$ term. At this point, additional Si doping produces acceptors as well as donors. As the compensation ratio approaches unity ($\gamma \rightarrow 1$), additional Si doping is predicted to incorporate equally as donors and acceptors effectively limiting the electron concentration.

Defining $n = n_{sat}$ when $\gamma = 1$ in Eq. (14) and solving for n_{sat} gives

$$n_{sat} = n_i\cdot\{K_c(T)\cdot[V_{Ga}^{-}]/[V_{As}^{+}]\}^{1/4}. \qquad (15)$$

Thus, the saturated electron concentration can be shown to depend upon terms which are temperature dependent. In addition, this saturation value increases with the fourth root of the ratio of vacancy concentrations. At a fixed temperature it is possible to vary this ratio by changing annealing or epitaxial growth conditions and thus influence the saturated electron concentration. However, the level of electron saturation is predicted to be weakly dependent on these conditions. For example, the ratio of Ga to As vacancy concentrations must be changed by a factor of 16 to produce a factor-of-2 change in the saturated electron concentration of Eq. (15).

The shape of this saturation versus Si concentration can be determined by solving for the room-temperature electron concentration, $n_{rt} = [Si_{Ga}^{+}] - [Si_{As}^{-}]$. This differs from n, the electron concentration at the annealing temperature, by

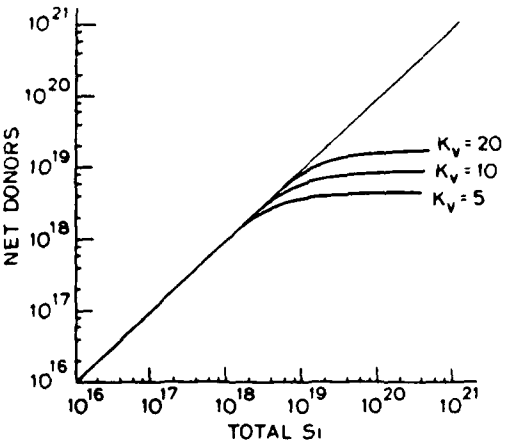

FIG. 5. Room-temperature electron concentration vs total dopant concentration calculated from Eq. (16) for various values of K_v.

the hole concentration, $p = n_i^2/n$. The hole concentration at room temperature can be ignored for most doping levels. The following relations between the electron concentration and the various Si species will be used:

$$n_{rt} = [\mathrm{Si}_{\mathrm{Ga}}^{+}] - [\mathrm{Si}_{\mathrm{As}}^{-}], \tag{16a}$$

$$n + [\mathrm{Si}_{\mathrm{As}}^{-}] = p + [\mathrm{Si}_{\mathrm{Ga}}^{+}], \tag{16b}$$

$$[\mathrm{Si}] = [\mathrm{Si}_{\mathrm{Ga}}^{+}] + [\mathrm{Si}_{\mathrm{As}}^{-}] + 2 \cdot [\mathrm{Si}_{\mathrm{Ga}} - \mathrm{Si}_{\mathrm{As}}], \tag{16c}$$

$$[\mathrm{Si}_{\mathrm{Ga}}^{+}] \cdot [\mathrm{Si}_{\mathrm{As}}^{-}] = K_p \cdot [\mathrm{Si}_{\mathrm{Ga}} - \mathrm{Si}_{\mathrm{As}}], \tag{16d}$$

$$n_{\mathrm{sat}}/n_i = (K_c \cdot [V_{\mathrm{Ga}}^{-}]/[V_{\mathrm{As}}^{+}])^{1/4} = K_v. \tag{16e}$$

Equations (16c) and (16d) include the contribution of Si nearest-neighbor pairs in the compensation process. Similar equations were used in Sec. III for the pair diffusion model. We will solve this set of equations for n_{rt} vs [Si] using different values of K_v in Eq. (16e). Note that we have ignored the contribution of the vacancies in the charge neutrality equation (16b). Vacancy concentrations are taken to be in the $10^{17}/\mathrm{cm}^3$ range or less and should be considered for Si concentrations in this range.

The solutions to Eqs. (16a)–(16e) are plotted in Fig. 5 for $K_v = 5,10,20$ with an intrinsic carrier concentration of $n_i = 1 \times 10^{18}/\mathrm{cm}^3$ corresponding to 1000 °C. In each curve, there is a sharp saturation at a level determined by K_v with negligible compensation for lower Si concentrations. From Eq. (14), we see that the compensation ratio for these low Si concentrations is equal to K_v^{-4}, which is nearly zero for the values of K_v in Fig. 5.

We have selected values of K_v that produce saturation curves typical of Si doping in GaAs. The direct calculation of K_v as a function of temperature and annealing conditions is beyond the scope of this paper. However, the solutions in Fig. 5 do suggest that the autocompensation of amphoteric dopants, driven by an increasing electron concentration, can account for the saturated free-electron concentrations widely observed in GaAs.[2,3,15–17]

VI. SUMMARY

The amphoteric nature of Si in GaAs has been used to develop diffusion and electrical compensation mechanisms. The diffusion mechanism is based on nearest-neighbor donor-acceptor pairs. General solutions were presented that predicted abrupt diffusion fronts for a wide range of pairing conditions. Experiments support the application of this mechanism to Si diffusion in GaAs at high concentrations.

A compensation mechanism for amphoteric dopants was developed as well. The compensation process is driven primarily by the free-electron concentration. Nearly complete compensation is predicted for large dopant concentrations.

ACKNOWLEDGMENTS

The authors wish to thank Dan Dobkin and Jim Harris for their helpful discussions. This work was supported by AROD (contract DAAG 29-81K-0061) and also by ARPA (contract NO0014-83-K-0363).

[1] L. J. Vieland, J. Phys. Chem. Solids **21**, 318 (1961).
[2] G. R. Antell, Solid-State Electron. **8**, 943 (1965).
[3] M. E. Greiner and J. F. Gibbons, Appl. Phys. Lett. **44**, 750 (1984).
[4] D. H. Lee, R. H. Malbon, and J. M. Whelan, in *Ion Implantations in Semiconductors* (Plenum, New York, 1976), p. 115.
[5] J. Kasahara, Y. Kato, M. Arai, and N. Watanabe, J. Electrochem. Soc. **130**, 2275 (1983).
[6] J. Kasahara and N. Watanabe, in *Semi-insulating III-V Materials* (Shiva, England, 1982), p. 115.
[7] T. Onuma, T. Hariao, and T. Sugawa, J. Electrochem. Soc. **129**, 837 (1982).
[8] H. C. Casey, Jr., in *Atomic Diffusion Semiconductors*, edited by D. Shaw (Plenum, New York, 1973), p. 351.
[9] K. K. Shih, J. W. Allen, and G. L. Pearson, J. Phys. Chem. Solids **29**, 379 (1968).
[10] J. Gyulai, J. W. Mayer, I. V. Mitchell, and V. Rodriguez, Appl. Phys. Lett. **17**, 332 (1970).
[11] K. Koyama, K. Takasaki, M. Maeda, and M. Takagi, Extended Abstracts of the Electrochemical Society Fall Meeting, Denver, CO, 11–16, October 1981, p. 738.
[12] J. K. Kung and W. G. Spitzer, J. Appl. Phys. **45**, 4477 (1974).
[13] R. M. Logan and D. T. J. Hurle, J. Phys. Chem. Solids **32**, 1739 (1979).
[14] H. R. Potts and G. L. Pearson, J. Appl. Phys. **37**, 2098 (1966).
[15] D. E. Davies, P. J. McNally, J. P. Lorenzo, and M. Julian, IEEE Electron Device Lett. **EDL-3**, 102 (1982).
[16] Y. G. Chai, R. Chow, and C. E. C. Wood, Appl. Phys. Lett. **39**, 800 (1981).
[17] J. S. Harris, Stanford Electronics Laboratory (private communication).
[18] P. Pianetta, J. Amano, G. Woolhouse, and C. A. Stolte, in *Materials Research Society Symposia Proceeding* (Elsevier North-Holland, New York, 1981), Vol. I, p. 239.

REGROWTH OF AMORPHIZED COMPOUND SEMICONDUCTORS

W.G. OPYD * and J.F. GIBBONS
Stanford Electronics Laboratories, Stanford University, Stanford, CA 94305
*Also Lockheed Research and Development Division, Palo Alto, CA 94304

ABSTRACT

Epitaxial regrowth is investigated for layers of InSb and GaAs amorphized by liquid nitrogen temperature ion implants. Experimental criterion for amorphization and limitation of regrowth are correlated with damage calculated by a Boltzmann transport equation approach to ion implant modeling. Conditions for complete epitaxial regrowth as determined by channeled Rutherford backscattering spectrometry are presented with evaluation of residual defects by transmission electron microscopy. Electrical activation following regrowth of GaAs is reported and correlated with calculated damage profiles.

INTRODUCTION

An understanding of defects resulting from ion implant damage in compound semiconductors is vital to employing ion implantation effectively for IR detector arrays and high-speed, high-density III-V integrated circuits. A technique has been developed by Christel [1] for the modeling of lattice displacements and stoichiometric imbalances resulting from implant damage in compound semiconductors. This technique, the Boltzmann transport equation (BTE) approach to ion implantation in multilayered structures and compound semiconductors, is used in this work to correlate experimental observations with physical damage mechanisms. Damage profiles from Rutherford backscattering spectrometry (RBS) and transmission electron microscopy (TEM) are correlated with features of BTE calculations to develop a physical understanding of the defect formation processes and allow for prediction of results over a spectrum of implant parameters.

The particular application of correlation of experiment with BTE calculations addressed in this work is the amorphization and solid phase epitaxial regrowth of compound semiconductors. The motivation for an amorphizing ion implant followed by solid phase epitaxy (SPE) is that it has been known for some time [2] that in silicon this technique results in activation of implanted dopants at significantly lower temperatures (<600°C) than those required to remove implant defects when the target is not amorphized. The lower temperature required for the anneal and activation of an amorphizing implant would be attractive for compound semiconductor devices from the standpoint of minimizing material decomposition as well as reducing impurity redistribution, which degrades the definition of device geometries. SPE of GaAs following amorphization was demonstrated by Williams and Austin [3] and has recently been investigated by others [4-7] but electrical activation has not been reported. In the following sections amorphization criteria are proposed for InSb and GaAs followed by observations on the correlation of SPE results with BTE calculations.

AMORPHIZATION

Two models for the threshold of amorphization in column IV semiconductors have been proposed. These are the damage density model of Vook

Mat Res Soc Symp Proc Vol 45 1985 Materials Research Society

[8] and the lattice displacement model of Swanson et al. [9]. The damage density criterion proposes that the energy deposited in nuclear stopping processes must exceed a threshold value for amorphization to occur. For silicon, at sufficiently low temperature to avoid in-situ annealing, the threshold has been determined to be 6 to 10×10^{20} KeV/cm^3 [8]. The lattice displacement criterion proposes that the lattice will relax to an amorphous phase when a specific fraction of the lattice has been displaced. Swanson [9] has calculated a lattice displacement threshold of 2 to 4% for Ge and Christel [10] has determined a threshold of 10% for Si by correlation of BTE calculations with experiment.

Profiles of damage density and lattice displacement as calculated by the BTE approach have been compared with the results of amorphizing implants into InSb and GaAs. An example of this correlation is shown in Fig. 1 for a 280KeV Cd implant into InSb. Channeled RBS spectra were used to determine amorphous layer thickness. For these measurements 2.2MeV He^+ particles were channeled in the (111) InSb and (100) GaAs. The damaged layer is indicated by a high yield of backscattered He^+. The He^+ were detected at an angle of 5 degrees from the surface for shallow implants to enhance depth resolution. Comparing similar calculations for Cd implants into InSb at energies ranging from 100 to 280KeV and doses of 10^{13} to 10^{14} ions/cm^2, the damaging energy density necessary for complete amorphization of InSb was found to lie in the range of 2 to 3×10^{20} KeV/cm^3. The fact that this value is less than that observed for Si is consistent with the cohesive energy of InSb bonds (1.4eV) being less than cohesive bond energy of Si (2.3eV) [11]. The damage density threshold for GaAs has been determined to be on the order of 1.5 to 11×10^{20}KeV/cm^3 for Si implants at 50 to 150KeV. The cohesive bond energy of GaAs is reported to be 1.6eV [11]. For the lattice displacement calculation a value must be assumed for the energy necessary to displace an atom from its lattice site which would correspond to four cohesive bond energies [10].

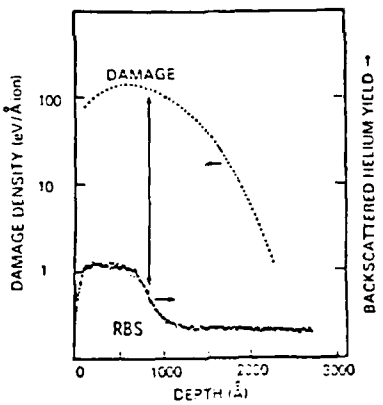

Figure 1 Correlation of amorphous layer thickness measured by RBS with damage density computed by the BTE approach for a 280KeV/ 3×10^{13} Cd implant into InSb.

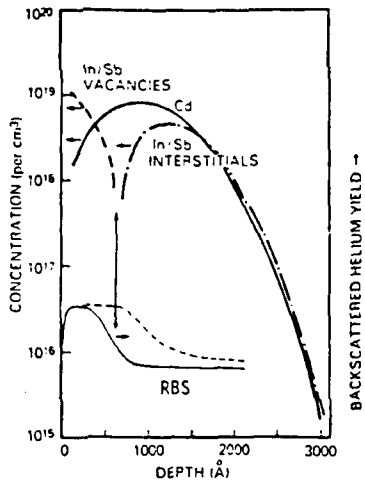

Figure 2 Correlation of RBS of InSb damaged layer as implanted and after anneal with BTE calculations of damage profiles.

Correlation of BTE calculations with RBS measurements of amorphous layer thickness results in a lattice displacement criterion of 2 to 3% for InSb and 3 to 16% for GaAs using 5.6eV and 6.4eV, respectively, for displacement energies.

Both the damage density and lattice displacement thresholds determined for GaAs vary by nearly an order of magnitude. This is believed to be the result of annealing occurring during implantation though all implants were done at liquid nitrogen temperature in order to minimize this effect. As discussed by Vook and Stein [12], the production rate of defects in the approach to the amorphous transition is the result of a balance between the introduction by the ion flux and the removal by thermal annealing processes. A complicating consideration is that while an increase in ion dose rate will increase the defect introduction rate linearly, it will also cause target heating which can have an exponential effect on the defect removal rate.

SOLID PHASE EPITAXY

After rendering an InSb or GaAs surface layer amorphous, SPE was performed to recover the crystal structure. RBS spectra for InSb before and after regrowth are shown in Fig. 2 below calculated damage profiles. In this case regrowth is not complete, stopping near the depth at which a transition occurs from net excess In and Sb to net vacancies. For Cd implants at 100, 220 and 280 KeV regrowth appeared to start rapidly (>1 Angstrom/sec) and then stop (<.01 Angstrom/sec) after 30s at 280C. Correlating the depth at which regrowth stops with BTE calculations, indicates that this occurs at a net vacancy concentration on the order of $10^{18}cm^{-3}$. A stopping of the regrowth due to vacancies indicates a limitation of diffusion of In and Sb from the depths to which they are recoiled, out to the near surface region of net vacancies. This limitation in the rate of SPE could permit time for nucleation of crystallites at the surface or within the damaged layer. This could stop SPE short of reaching the surface as shown by Williams et al. [13]. Random orientation of these crystallites would cause the damaged layer to regrow in a polycrystalline structure. The slope of the deep damage edge in the RBS data of Fig. 2 would support the argument of crystallite formation. The slope of the edge before anneal is consistant with an abrupt amorphous edge convolved with the system resolution and energy straggle. In the post-anneal case, however, the slope indicates that the transition is no longer abrupt but graded due to the nucleation of misoriented crystallites.

Regrowth experiments on GaAs also demonstrated a nonlinear growth rate characterized by initial rapid growth that slows and then stops at a given anneal temperature. Figure 3 shows RBS data for GaAs as amorphized with Si at 50KeV and regrown at 550C. In addition to regrowth stopping after 10 minutes at 550C, arsenic loss near the surface can be observed as indicated by the lower RBS yield at the surface in the post-anneal channeled spectrum and random spectrum (not shown). To prevent arsenic loss during the anneal a thin film of aluminum was evaporated onto the surface of a sample that was then processed with the same implant and anneal conditions. The aluminum encapsulated sampled regrew completely as indicated by the RBS data of Fig. 3 showing the post-anneal spectrum coincident with the spectrum for unimplanted material. Plan view bright field TEM and electron diffraction patterns are shown for the aluminum capped sample as-implanted and after anneal in Fig. 4(a) and 4(b), respectively. In the as-implanted case amorphous rings are observed in the diffraction pattern superimposed on the pattern for the (100) substrate.

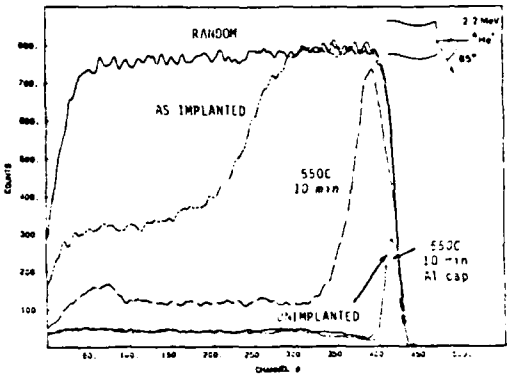

Figure 3 Channeled RBS spectra for GaAs amorphized by 50KeV Si and regrown at 550C for 10 min.

After the anneal, residual dislocation loops are apparent. BTE calculations of recoil and damage profiles for the aluminum capped sample are shown in Fig. 5. It may be noted that this condition in which complete regrowth was achieved corresponds to no net vacancies near the surface due to aluminum recoils.

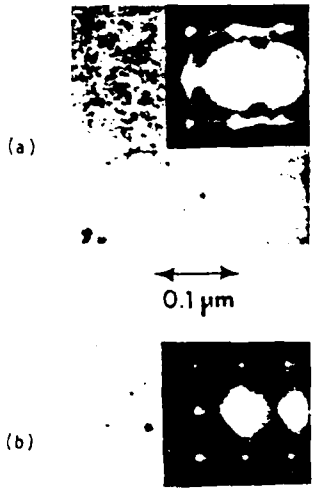

Figure 4 Plan-view bright-field TEM and electron diffraction patterns for GaAs (a) as implanted and (b) after 550C for 10 min.

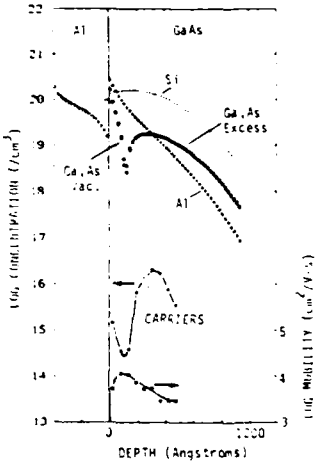

Figure 5 Correlation of electrical activation profiles of regrown GaAs with BTE calculations of recoil profiles

Electrical activation analysis by van der Pauw-Hall measurements were performed on an aluminum capped sample of (100) undoped, LEC GaAs and the results are shown in Fig. 5. A low level of n-type electrical activation was observed to the depth of the initial amorphous layer indicating that some of the implanted Si replaced Ga atoms in the low temperature regrowth process. The level of activation near the surface is suppressed, possibly due to Al preferentially growing onto Ga sites as opposed to Si in this region where Al concentration is high. The high mobility observed is consistent with a low concentration of residual electrically active defects.

CONCLUSION

Amorphization by ion implantation and subsequent SPE of InSb is reported for the first time. The threshold for amorphization of InSb and GaAs in terms of damage deposited in nuclear stopping processes has been determined by correlating RBS measurements to BTE calculations of damage. A limitation of SPE in GaAs and InSb appears to be correlated with the transition from a net excess deep in the implanted material to net vacancies near the surface. This atomic imbalance is due to recoils. GaAs layers under an Al cap have been amorphized and regrown completely. In this case, Al recoiled into the GaAs compensates for Ga and As displaced near the surface to result in no net atomic vacancies. A low level of n-type electrical activation was observed in the regrown GaAs with mobility indicative of few residual electrically active defects. With the implant damage removed by the low temperature regrowth a rapid anneal could be employed for further Si activation.

ACKNOWLEDGMENTS

The authors are grateful for the support of this work by ARO contract DAAG-29-81-K-0061 and Lockheed independent research funds. They also wish to acknowledge H. Kawayoshi of ARACOR for TEM services.

REFERENCES

1. L. A. Christel and J. F. Gibbons, J. Appl. Phys. 52, 5050 (1981).
2. B. L. Crowder, J. Electrochem. Soc. 117, 671 (1970).
3. J. S. Williams and M. W. Austin, Appl. Phys. Lett. 36, 994 (1980).
4. M. G. Grimaldi, B. M. Paine, M-A. Nicolet and D. K. Sadana, J. Appl. Phys. 52, 4032 (1981).
5. Y. I. Nissim, Stanford University Ph.D. dissertation, June 1981.
6. R. S. Bhattacharya, A. K. Rai, Y. K. Yeo, P. P. Pronko, S. C. Ling, S. R. Wilson and Y. S. Park, J. Appl. Phys. 54, 2329 (1983).
7. D. K. Sadana, T. Sands and J. Washburn, Appl. Phys. Lett. 44, 301 (1984).
8. F. L. Vook, Radiation Damage and Defects in Semiconductors. (London Institute of Physics, 1972) p. 60.
9. M. L. Swanson, J. R. Parsons and C. W. Hoelke, Rad. Effects 9, 249 (1971).
10. L. A. Christel, J. F. Gibbons and T. W. Sigmon, J. Appl. Phys. 52, 7143 (1981).
11. W. A. Harrison, Electronic Structure and the Properties of Solids, W. H. Freeman, San Francisco (1980) p. 176.
12. F. L. Vook and H. J. Stein, Rad. Effects 2, 23 (1969).
13. J. S. Williams, F. M. Adams and K. G. Rossiter, Thin Films and Interfaces, P. S. Ho and K. N. Tu, eds., North-Holland, New York (1982) p. 183.

Paper #3

Damage calculation and measurement for GaAs amorphized by Si implantation

W. G. Opyd
Lockheed Research and Development Division, Palo Alto, California 94304

J. F. Gibbons
Stanford Electronics Laboratories, Stanford University, Stanford, California 94305

J. C. Bravman and M. A. Parker
Materials Science and Engineering, Stanford University, Stanford, California 94305

(Received 23 June 1986; accepted for publication 14 August 1986)

Extended defects in GaAs are investigated following epitaxial regrowth of amorphous layers. GaAs surface layers were amorphized by Si^+ implants at liquid-nitrogen temperature. Anneals were performed for 4 s to 30 min from 150 to 885 °C. Rutherford backscattering spectrometry and transmission electron microscopy were used to evaluate the results of annealing. Complete solid-state epitaxy occurs rapidly at low temperature. Stacking faults and microtwins surrounded by dislocation networks extend to the surface following regrowth. The dislocations anneal at varying rates over intermediate temperature ranges (200–700 °C), and the microtwins climb out at higher temperatures (> 700 °C). Defect depth profiles are correlated with damage and stoichiometric imbalances computed by the Boltzmann transport equation approach to ion-implant modeling.

It is well known that solid phase epitaxy (SPE) at a relatively low temperature (~ 600 °C for a Si crystal) permits ion-implanted dopants to be incorporated into substitutional sites in a Si crystal. This process was first demonstrated for silicon by Crowder in 1970.[1] For the compound semiconductor GaAs a low-temperature process for impurity incorporation is attractive because it provides both reduced material decomposition and reduced impurity redistribution during annealing. SPE of GaAs was demonstrated by Williams and Austin in 1980[2] and has recently been investigated by others.[3-7] Although SPE in GaAs has been demonstrated at very low temperatures[2] (180 °C), extended defects are often observed in the implanted layer following SPE. In this letter, Rutherford backscattering spectrometry (RBS) and high resolution transmission electron microscopy (HRTEM) results for Si-implanted GaAs are presented with a correlation to lattice damage calculated by the Boltzmann transport equation (BTE) approach to ion implantation modeling.[8-10] Based on this correlation a source of microtwin nucleation is presented, extrinsic dislocation loops are tentatively identified, and an amorphization threshold is derived.

Silicon ions were implanted into undoped semi-insulating liquid encapsulated Czochralski (100) GaAs to a dose of 10^{15} cm^{-2} at 100 keV. The GaAs target was cooled to liquid-nitrogen temperature during implantation to minimize *in situ* annealing. After rendering a GaAs surface layer amorphous, SPE was performed to recover the crystal structure. Anneals were conducted over a temperature range of 150–885 °C in forming gas. Anneal times ranged from 4 s to 30 min. For HRTEM analysis cross-sectional specimens were prepared by a technique similar to that described by Bravman[11] with modificat ons to minimize specimen heating which could lead to unwanted annealing.

Depth profiles of the BTE calculations for displaced Ga or As atoms, shown at the top of Fig. 1, are computed to be more than an order of magnitude greater than the Si concentration over much of the profile. Although computed profiles for Ga and As differ slightly due to their difference in mass, they are shown in Fig. 1 as a single curve since differences are generally less than a few percent. The profile of Ga or As displaced was calculated assuming a 10-eV displacement energy. Though the appropriate value for displacement energy is subject to speculation, use of 5 and 20 eV was found to result in only a 20% change in the displacement concentration profile. The recoiling of Ga and As from the near-surface region results in a net vacancy concentration there while Ga and As atoms pile up deeper into the substrate producing a local net excess. Due to the difference in Ga and As masses, the Ga atoms are recoiled further, resulting in the surface region being slightly As rich while the deeper region is slightly Ga rich.

Transmission electron microscopy (TEM) on the As-implanted material shown in Fig. 2 reveals an amorphous region extending from the surface to a depth of 950 Å. The amorphous region was indicated by an absence of thickness contours on tilting the specimen and by the rings in the selected area diffraction pattern. From 950 to 1250 Å a heavily defected transition region is observed to occur between the amorphous layer and the single crystal bulk. The threshold for amorphization was determined in terms of two BTE criteria. Comparing the depth of the transition region to the computed displacement profile indicates that the fractional lattice displacement necessary for a crystalline to amorphous transition in GaAs is in the range of 18–25%. A similar correlation was made with a computed profile of the energy deposited in nuclear stopping processes, indicating an amorphization threshold in terms of this criterion of 1.1–1.7×10^{21} keV/cm^3. This corresponds to 50–77 eV per GaAs molecule for Si implantation, significantly higher than the 11 ± 2 eV reported by Sands *et al.* for Se implantation.

Following SPE, the near-surface region is seen to be

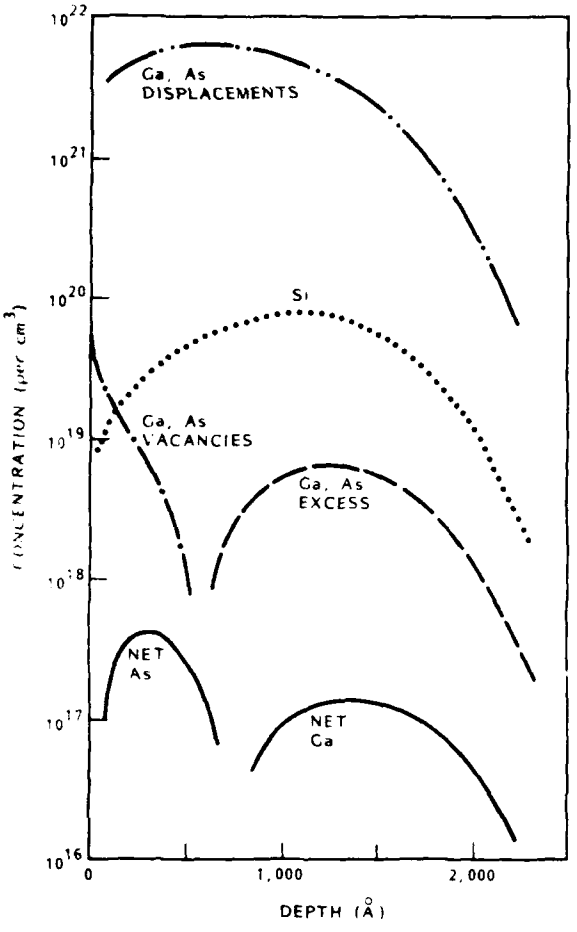

FIG. 1. Depth profiles of Boltzmann transport equation calculations for a 10^{15} Si/cm^2 implant at 100 keV into GaAs.

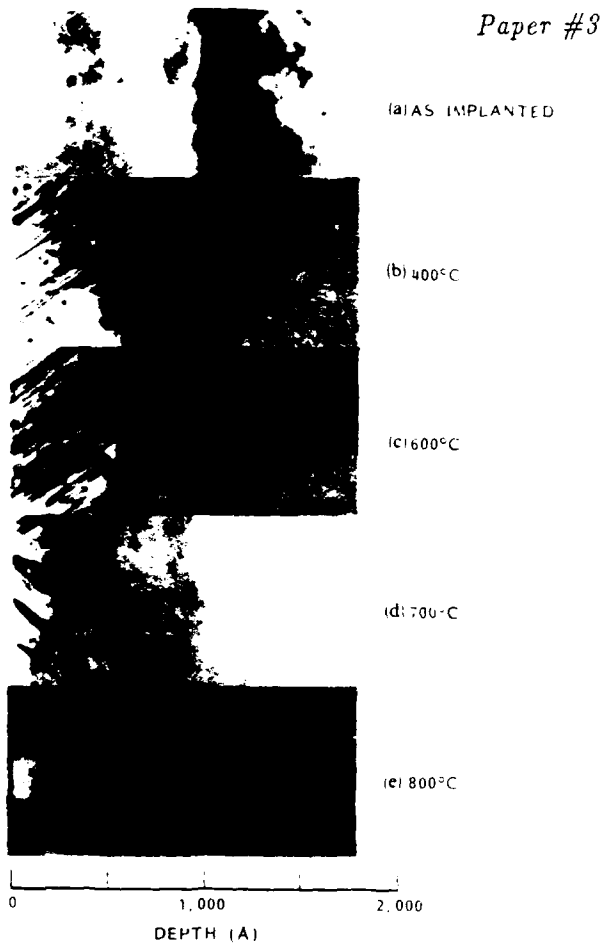

FIG. 2. Cross-sectional TEM of GaAs (a) as implanted with 100 keV Si to a dose of 10^{15} cm^{-2} and after anneals of (b) 400 °C for 10 s, (c) 600 °C for 30 s, (d) 700 °C for 30 s, and (e) 800 °C for 30 s.

highly defected in the cross-sectional TEM of Fig. 2. The selected area diffraction pattern indicates the regrowth was complete but a high density of stacking faults and microtwins remain. Stacking faults were indicated by the streaks in the diffraction pattern and microtwins were indicated by the faint diffracted beams displaced one-third of the distance between primary diffracted beams.

A lattice image for this specimen is shown in Fig. 3 viewed in a (110) direction. For this image four 111 and two 200 reflections were used in conjunction with the undiffracted beam. Here microtwins are clearly evident with their characteristic boundaries on (111) facets intersecting the (100) material surface at an angle of 54.7°. The HRTEM demonstrates that crystal recovery with low defect densities occurs in the transition region. In regrowth of the amorphous region, however, stacking faults and microtwins nucleate and propagate to the surface.

Although the average net Ga and As concentrations are too low to account for sufficient antisite defects to nucleate all the stacking faults observed, local variations in the stoichiometry around damage clusters could account for this. BTE calculations indicate that greater than 99% of the displaced atoms at the amorphous to crystalline interface recoil less than 5 Å. The density of stacking faults and microtwins in the regrown region does correlate with the high density of total displacements. A high density of residual dislocation loops is observed in TEM of the completely regrown material. The depth at which these are observed correlates with the Si peak and the net Ga and As excess in the BTE calculations, indicating that these may be extrinsic loops formed by Si, Ga, and As precipitation.

Channeled RBS spectra are shown in Fig. 4 for anneals at 600, 700, and 800 °C. These anneals were intended to remove residual defects following SPE at 400 °C for 10 s. The depth scale shown, though based on a surface approximation of electronic stopping power, correlates well with cross-sectional TEM. An anneal at 600 °C for 4 s resulted in both a reduction in the depth to which the damage extends and a reduction in the height of the near-surface yield. Anneals for longer times at 600 °C can be seen to further reduce the depth to which the damage extends, but at a much lower rate and with no noticeable change in near-surface yield. The anneals at 600, 700, and 800 °C for 30 s can be seen to result in successively lower near-surface yields. A channeled RBS spectrum indistinguishable from the unimplanted spectrum was achieved after 800 °C for 30 min in an arsine atmosphere.

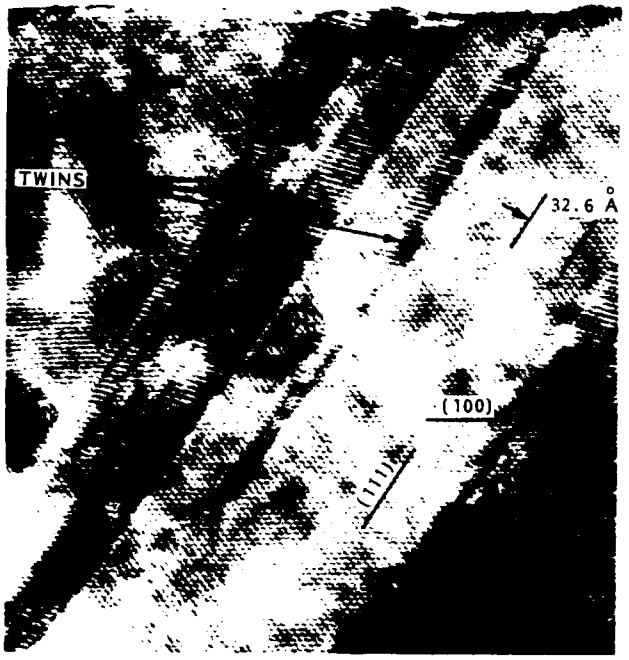

FIG. 3. Lattice image of GaAs following amorphization and regrowth showing microtwins extending to the surface.

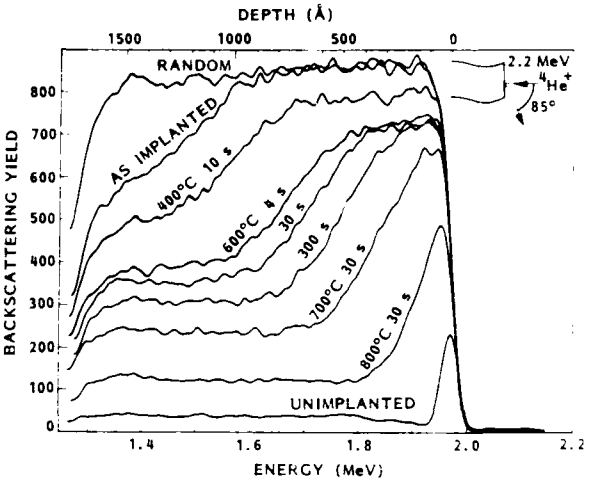

FIG. 4. Channeled RBS spectra for GaAs amorphized by Si implantation and annealed at 400, 600, 700, and 800 °C.

Following SPE the lowering of the height of the RBS yield at temperatures of 200–600 °C is believed to be due to the removal of dislocation networks and of faults within them. A variety of dislocation network sizes and configurations results in arrays that require varying temperatures for removal. This would account for a near-surface yield that is temperature dependent. Complete removal of defects accounting for the near-surface yield does not occur unless the temperature is increased to the range of 700 °C. This appears to be due to the thermal energy required for removal of the microtwins that intersect the surface.

In conclusion, a correlation of BTE calculations with RBS and TEM results has been used to determine the fractional displacement of Ga and As atoms necessary for the crystalline to amorphous transition in GaAs at liquid-nitrogen temperature. BTE calculations of damage profiles are also presented and correlated with stacking faults and microtwins observed in TEM results. Finally, RBS data for a GaAs anneal sequence are correlated with TEM observations to identify defects responsible for the RBS yield and to determine how they anneal. Although many stacking faults and dislocations are removed at lower temperatures, temperatures in the range of 700 °C are required for complete microtwin removal. For this reason, amorphization followed by SPE as a low-temperature doping technique will be applicable only to conditions in which the precipitation of dislocation and microtwin nuclei can be suppressed as was apparently the case for the low-energy shallow implant reported previously.[12]

We would like to thank A. F. Marshall for assistance in TEM and acknowledge support for this work at Lockheed by independent research funds and at Stanford by the Army Research Office under contract DAAG29-85-K-0054. This work has benefited from facilities made available through the National Science Foundation Materials Research Laboratory program through the Center for Materials Research at Stanford.

[1] B. L. Crowder, J. Electrochem. Soc. **117**, 671 (1970).
[2] J. S. Williams and M. W. Austin, Appl. Phys. Lett. **36**, 994 (1980).
[3] M. G. Grimaldi, B. M. Paine, M. A. Nicolet, and D. K. Sadana, J. Appl. Phys. **52**, 4032 (1981).
[4] A. K. Rai, R. S. Bhattacharya, P. P. Pronko, and S. C. Ling, J. Appl. Phys. **54**, 2307 (1983).
[5] D. K. Sadana, T. Sands, and J. Washburn, Appl. Phys. Lett. **44**, 623 (1984).
[6] T. Sands, D. K. Sadana, R. Gronsky, and J. Washburn, Appl. Phys. Lett. **44**, 874 (1984).
[7] C. Liccope, Y. I. Nissim, and C. Meriadec, J. Appl. Phys. **58**, 3094 (1981).
[8] L. A. Christel and J. F. Gibbons, J. Appl. Phys. **52**, 5050 (1981).
[9] L. A. Christel, J. F. Gibbons, and T. W. Sigmon, J. Appl. Phys. **52**, 7143 (1981).
[10] M. D. Giles and J. F. Gibbons, IEEE Trans. Electron Devices **ED-32**, 1918 (1985).
[11] J. C. Bravman and R. Sinclair, J. Electron Microsc. Tech. **1**, 53 (1984).
[12] W. G. Opyd and J. F. Gibbons, Mat. Res. Soc. Symp. Proc **45**, 273 (1985).

Precipitation of Impurities in GaAs Amorphized by Ion Implantation

W.G. Opyd
Lockheed Research and Development Division, Palo Alto, California 94304-1187

J.F. Gibbons
Stanford Electronics Laboratories, Stanford University, Stanford, California 94305

A.J. Mardinly
Lockheed Missiles and Space Company, Sunnyvale, California 94088-3504

Abstract

Impurities, in a GaAs layer that had been amorphized by ion implantation, were observed to precipitate upon annealing. Photoluminescence spectra indicated that the resulting high electrical resistivity could be attributed to the formation of neutral impurity complexes rather than a compensation mechanism. Impurities studied were implanted Si and Se. Transmission electron microscopy and x-ray microanalysis were used to identify impurity precipitates and related stacking fault tetrahedra. These results correlate with similar examples of poor activation for impurities in GaAs grown by low temperature molecular beam epitaxy.

There has been interest for several years in the solid phase epitaxy (SPE) of a GaAs layer amorphized by ion-implantation. Interest was originally stimulated by the discovery that SPE at a relatively low temperature (600°C for a Si crystal) permits ion-implanted dopants to be incorporated onto substitutional sites in a Si crystal [1]. For the compound semiconductor GaAs a low temperature process for impurity incorporation is attractive because it provides both reduced material decomposition and reduced impurity redistribution during annealing. In addition, an impurity implanted into a preamorphized layer would have a relatively abrupt depth profile, without the deep channeling tail typical of implants into crystals [2]. SPE of GaAs was first demonstrated by Williams and Austin in 1980 [3] and has recently been investigated by others [4-10]. Although SPE in GaAs has been demonstrated at very low temperatures [3] (180°C), extended defects are often observed in the implanted layer following SPE. The extended defects have been reported to anneal at higher temperatures [10] but no significant electrical activation has been attained [2,11]. In this letter, the results of an investigation into the cause of poor electrical activation are presented, indicating that amorphization by ion implantation may be an effective means of producing an electrically inactive layer in GaAs.

The approach to the investigation into electrical activation was to implant known n-type impurities into a GaAs wafer, half of which had been preamorphized by arsenic implantation. After anneals of various times, temperatures and ambients, Hall measurements were performed for electrical activity, secondary ion mass spectroscopy (SIMS) was used to determine chemical depth profiles, photoluminescence (PL) was used to investigate impurity site location, transmission electron microscopy (TEM) was used for defect structure identification, and energy

dispersive x-ray microanalysis (EDX) was used for analyzing defect structure chemical composition.

Arsenic ions were implanted into undoped semi-insulating (SI) liquid encapsulated Czochralski (LEC) (100) GaAs to a dose of $3x10^{14}$ cm^{-2} at 100keV. This produced an amorphous layer of 800 Å as confirmed by TEM. Half of the wafer was masked from this amorphizing implant but not from the subsequent impurity implant so that chemical depth profiles and electrical activation could be compared for the two cases. The implants were intentionally shallow to emphasize the difference in the two halves of the wafer due to channeling in the side without the arsenic implant. The impurity implants tested were Si at 25keV and Se at 50keV, both to doses of 10^{13} cm^{-2}. These resulted in similar chemical depth profiles with SIMS data for Si shown in Fig. 1. Rapid thermal anneals (RTA) were used for SPE and defect removal to minimize thermal exposure. Though tests have been performed with arsenic ambients and various capping layers, the data presented is primarily for an ambient of forming gas with a silicon proximity cap.

Electrical activation, as measured by the van der Pauw-Hall technique, resulted in no n-type electrical activity for the Si in preamorphized GaAs following anneals up to temperatures at which conversion to p-type is expected [12]. The percent activation as a function of anneal temperature for a RTA of 5 s is shown in Fig. 2 for the crystalline and amorphous cases. The maximum activation for the crystalline case is low as expected due to the high doping level, in excess of 10^{18} cm^{-3}.

To see if the lack of n-type activity was due to compensating defects that require anneal temperatures in excess of the temperature at which type conversion occurs for Si doping, Se doping was attempted since it is known to activate well at higher temperatures. Though type conversion was not observed for the Se implants, the preamorphized material showed no activation while the crystalline control activated as expected for anneals of 1000°C to 1100°C for 3 s.

In an attempt to determine the site location of the implanted Si, PL measurements at 12°K were performed for wavelengths of 8000 to 11000 Å with a resolution of 7 Å. The PL spectra shown in Fig. 3 demonstrate effects in the region of a broad luminescence line attributed to a carbon donor-acceptor pair recombination [13]. As anneal temperature is increased, the lines for the preamorphized and unimplanted samples show no significant change, while the Si implant into crystalline GaAs shows a line developing at 8350 A that has been attributed to Si on an As site [12,13]. This represents the expected shift of the Si from Ga to As sites which has been used to explain the type conversion [12]. The absence of the Si impurity lines, however, has been used as an indication that the Si is complexed into an electrically inactive defect structure and not simply compensated by impurities of the opposite type[13].

In order to identify the defect structure that may be preventing the impurities implanted into preamorphized GaAs from activating, high resolution TEM was performed on cross-section specimens. A TEM micrograph of the GaAs viewed in a <110> direction and with lattice resolution is shown in Fig. 4 for a specimen implanted with Si and annealed at 1050°C for 3 s. Defects identified were stacking fault tetrahedra (SFT) and precipitates. Under the diffracting conditions of Fig. 4, these two structures may appear distinct, but upon closer analysis each precipitate was found to be associated with a SFT. The pricipitates were confirmed to contain Si by EDX measurements. Identical structures were noted for specimens in which Se had been implanted into the preamorphized GaAs. Precipitates at the core of SFTs have previously been noted to correlate with poor electrical activation and were attributed to local stoiciometric disturbances caused by an implant [14].

These results, indicating a lack of Si activation, correlate well with experiments on low temperature molecular beam epitaxy (LT-MBE) [15]. In .he LT-MBE case, activation of Si incorporated during growth was assumed dependent

upon the growth rate being slow enough to allow sufficient surface migration of the Ga and As to prevent local stoichiometric disturbances. If the growth rate was too fast, lack of activation was assumed to be due to compensation by acceptors but no evidence for this was given. A comparison of the rate for SPE [8] with the maximum LT-MBE rate for Si activation [15] is shown in Fig. 5. Though this comparison can not be made directly, since the LT-MBE is limited by surface migration while SPE is limited by bulk diffusion, it implies that activation of impurities in GaAs following SPE might not be expected.

In conclusion, impurities implanted into preamorphized GaAs have been shown to precipitate, inhibiting electrical activation. Though this conclusion rules out the use of implants into preamorphized GaAs for achieving abrupt doping profiles, it suggests a technique for producing electrically inactive material in spite of the presence of impurities. Amorphization of a layer of GaAs containing impurities would cause the local stoichiometric disturbances necessary to produce the defects that collapse into SFTs and precipitate the impurities.

We would like to thank L.J. Dries and S.K. Ichiki of Lockheed for assistance in PL and TEM work and W.S. Lee and J.S. Harris of Stanford for assistance in correlation with LT-MBE. This work was supported at Lockheed by independent research funds and at Stanford by the Army Research Office under contract DAAG29-85-K-0054.

References

1. B.L. Crowder, *J. Electrochem. Soc.* **117**, 671 (1970).

2. R.T. Blunt and P. Davies, *J. Appl. Phys.* **60**, 1015 (1986).

3. J.S. Williams and M.W. Austin, *Appl. Phys. Lett.* **36**, 994 (1980).

4. M.G. Grimaldi, B.M. Paine, M.A. Nicolet, and D.K. Sadana, *J. Appl. Phys.* **52**, 4032 (1981).

5. A.K. Rai, R.S. Bhattacharya, P.P. Pronko, and S.C. Lang, *J. Appl. Phys.* **54** 2307 (1983).

6. D.K. Sadana, T. Sands, and J. Washburn, *Appl. Phys. Lett.* **44**, 623 (1984).

7. T. Sands, D.K. Sadana, R. Gronsky, and J. Washburn, *Appl. Phys. Lett.* **44**, 874, (1984).

8. C. Licoppe, Y.I. Nissim, and C. Meriadec, *J. Appl. Phys.* **58**, 3094 (1985).

9. W.G. Opyd and J.F. Gibbons, *Mat. Res. Soc. Symp. Proc.* **45**, 273 (1985).

10. W.G. Opyd, J.F. Gibbons, J.C. Bravman, and M.A. Parker, *Appl. Phys. Lett.* **49**, 974 (1986).

11. R. Gwilliam, R.S. Deol, R. Blunt, and B.J. Sealy, *Mat. Res. Soc. Symp. Proc.* **92**, 437 (1987).

12. S.K. Tiku and W.M. Duncan, *J. Electrochem. Soc.* **132**, 2237 (1985).

13. J. Weber, S.J. Pearton, and W.C. Dautremont-Smith, *Appl. Phys. Lett.* **49**, 1181 (1986).

14. E. Morita, J. Kasahara, M. Arai, and S. Kawado, *Mat. Res. Soc. Symp. Proc.* **45**, 279 (1985).

15. G.M. Metze and A.R. Calawa, *Appl. Phys. Lett.* **42**, 818 (1983).

Figure Captions

1. Depth profile of implanted Si as determined by SIMS for implants into crystalline and amorphous GaAs.

2. Percent electrical activation of 10^{13} Si/cm^2 implanted at 25keV into crystalline and amorphous GaAs as a function of temperature for 5 s anneals.

3. Photoluminescence spectra of GaAs demonstrating the development of the Si on As site line with increasing anneal temperature for implants into crystalline material while this line is not present in preamorphized or unimplanted material.

4. High resolution TEM micrograph of Si implanted, preamorphized GaAs after an anneal of 1050°C for 3 s.

5. Comparison of the rate for SPE with the maximum rate of LT-MBE for which Si activation has been observed.

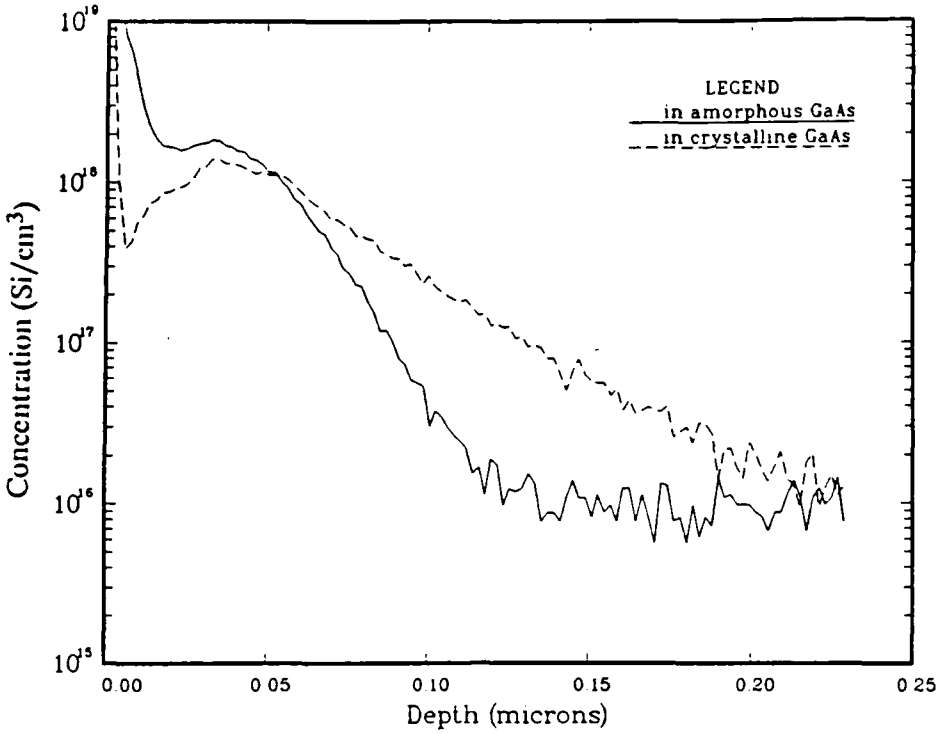
LEGEND
in amorphous GaAs
in crystalline GaAs
Concentration (Si/cm3)
Depth (microns)
0.00
0.05
0.10
0.15
0.20
0.25

Fig. 1

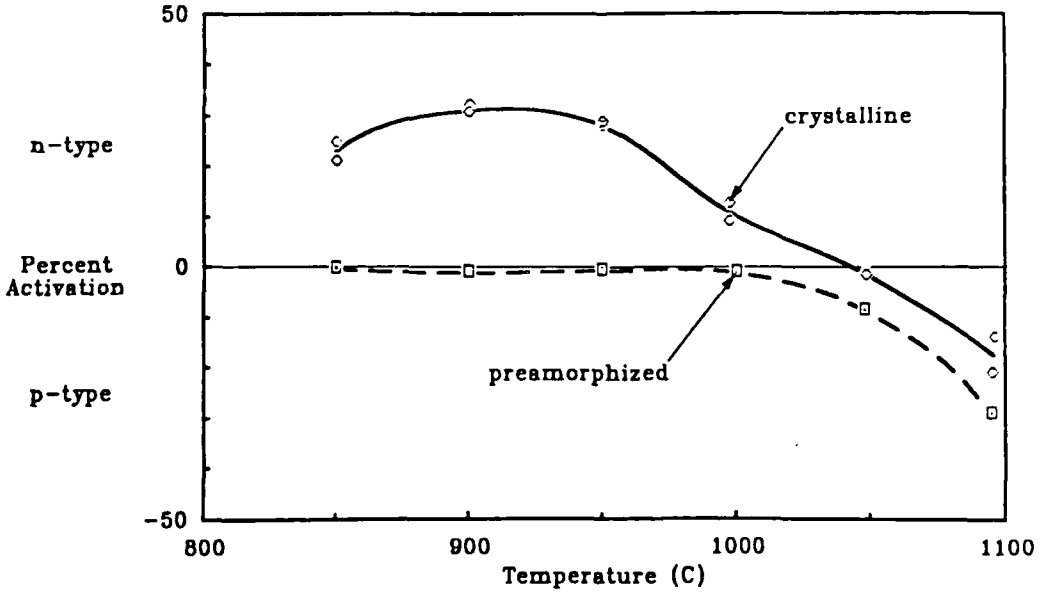
n-type
Percent Activation
p-type
50
0
-50
crystalline
preamorphized
800
900
1000
1100
Temperature (C)

Fig. 2

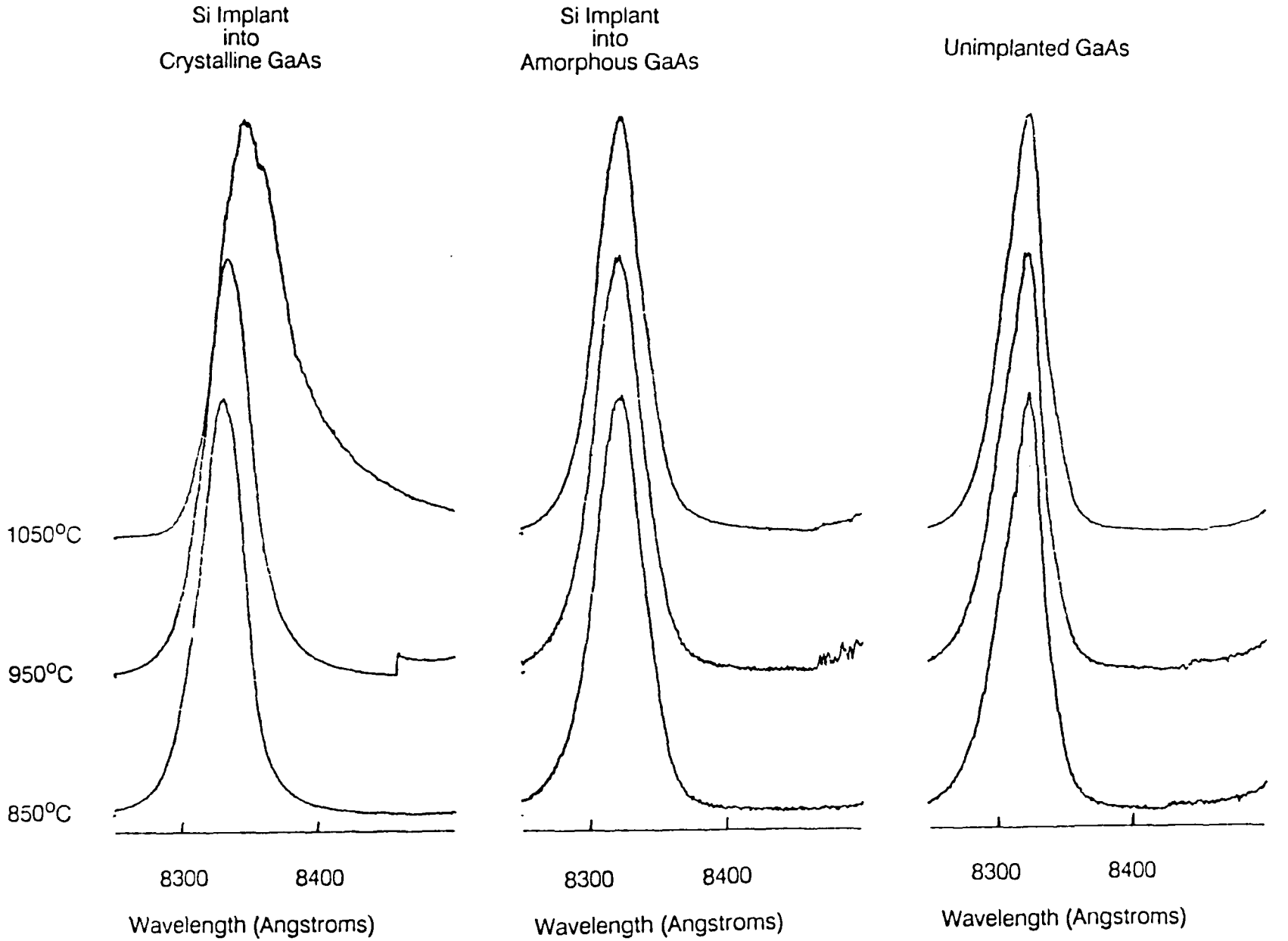
Si Implant
into
Crystalline GaAs
Si Implant
into
Amorphous GaAs
Unimplanted GaAs
1050°C
950°C
850°C
8300
8400
Wavelength (Angstroms)
8300
8400
Wavelength (Angstroms)
8300
8400
Wavelength (Angstroms)

Fig. 3

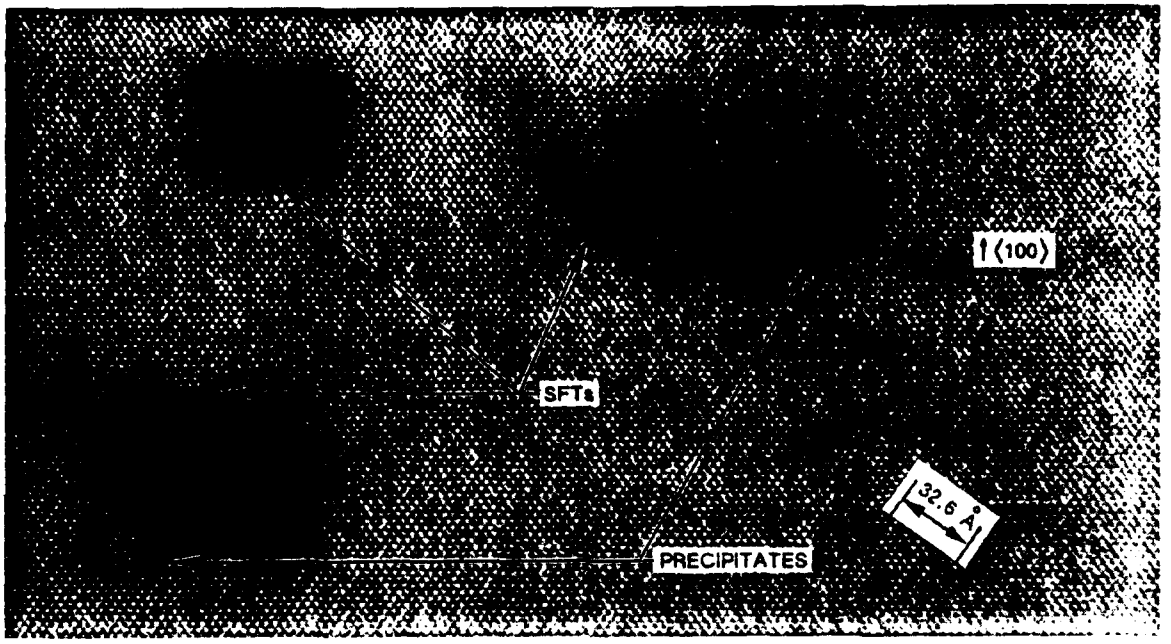

Fig.4

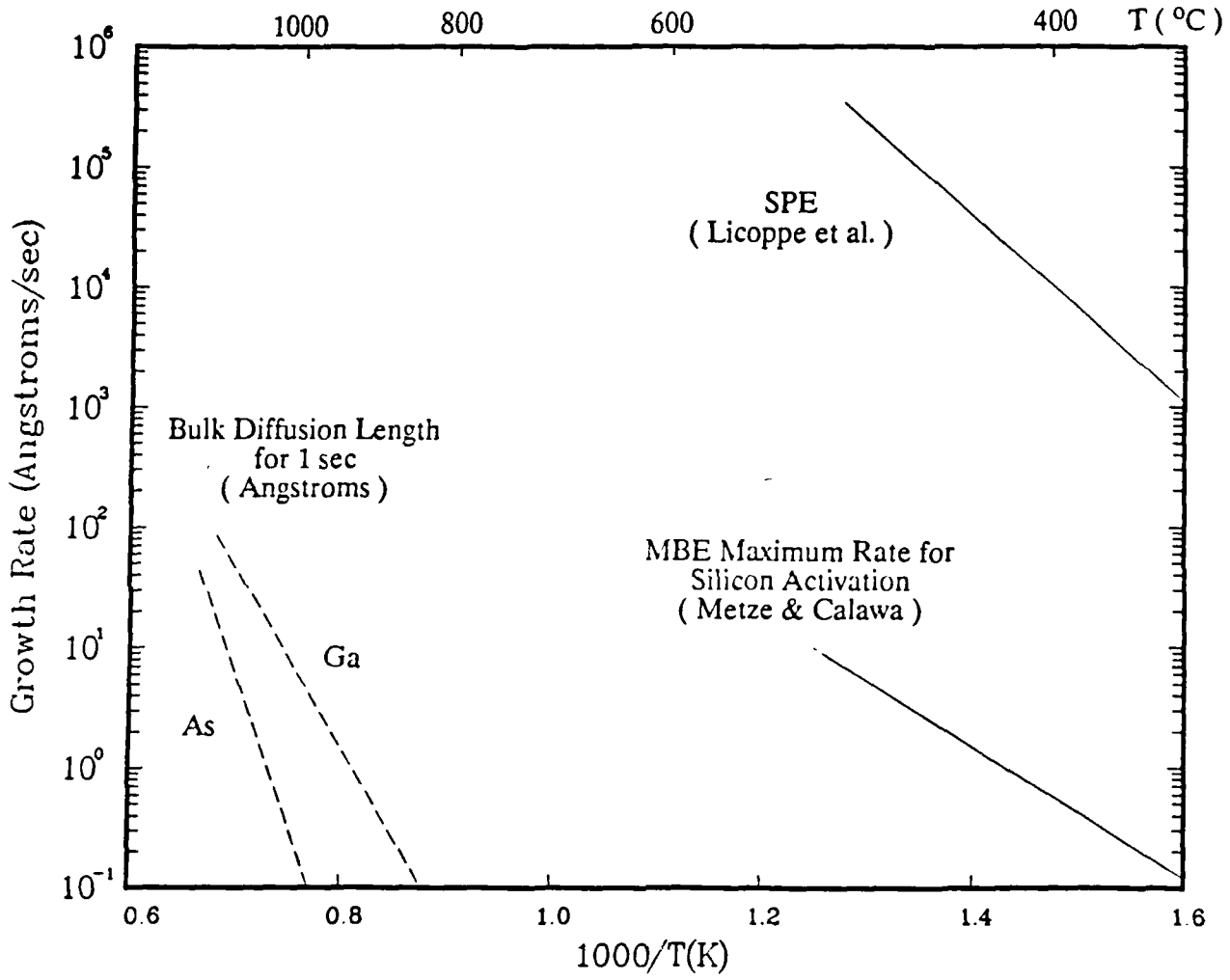
1000
800
600
400
T (°C)
10^6
10^5
10^4
10^3
10^2
10^1
10^0
10^{-1}
Growth Rate (Angstroms/sec)
SPE
(Licoppe et al.)
Bulk Diffusion Length
for 1 sec
(Angstroms)
MBE Maximum Rate for
Silicon Activation
(Metze & Calawa)
Ga
As
0.6
0.8
1.0
1.2
1.4
1.6
1000/T(K)

Fig. 5

Paper #5

Limited reaction processing: Growth of III-V epitaxial layers by rapid thermal metalorganic chemical vapor deposition

S. Reynolds, D. W. Vook, and J. F. Gibbons
Stanford University Electronics Laboratories, McCullough 226, Stanford, California 94305

(Received 6 October 1986; accepted for publication 28 October 1986)

We have demonstrated a new technique for III-V epitaxial layer growth combining rapid thermal processing and metalorganic chemical vapor deposition. This technique yields enhanced layer thickness control and abrupt interfaces while maintaining a high growth rate (>10 Å/s). Multilayer structures have been grown with smooth, featureless surfaces and good electrical quality ($N_d = 2\times10^{16}$ cm^{-3}, $\mu_n = 3000$ cm^2/V s) using trimethylarsenic and trimethylgallium.

The recent interest in GaAs and related III-V materials has been stimulated by the development of epitaxial growth techniques which yield materials of both good crystal and electrical quality along with tight control over layer thickness and interface abruptness. One of these techniques, metalorganic chemical vapor deposition (MOCVD), produces abrupt interfaces using elaborate and costly gas switching systems along with reduced reactor pressure. Recently, a new method of layer control has been demonstrated by Gibbons *et al.* for high quality thin layer growth of silicon layers with abrupt interfaces.[1,2] This method, limited reaction processing (LRP), uses rapid precise changes in the substrate temperature to switch layer growth on and off rather than relying on gas phase switching.

We report rapid thermal switched growth of GaAs epitaxial layers. We have extended this technique with equal success to $Al_xGa_{1-x}As$ ($0<x<0.25$) and $In_yGa_{1-y}As$ ($0<y<0.03$), all on GaAs substrates. Good electrical characteristics and surface morphology, featureless to within the resolution of our Nomarski microscope (1100×), have been consistently obtained. In contrast to standard MOCVD, this technique maintains a high growth rate (10 Å/s) at atmospheric pressure while producing abrupt interfaces.

Layers were grown using trimethylarsenic, trimethylgallium, trimethylaluminum, and triethylindium, all purchased from Alfa Products (Danvers, MA). Substrates, undoped and Si doped (100) Czochralski, were degreased and given a 5:1:1 H_2SO_4:H_2O_2:H_2O etch prior to loading. Optimum layers were grown at 670–720 °C with 3.5 l/min of total H_2 flow and a trimethylarsenic partial pressure of about 0.5 Torr. GaAs layers have *n*-type background doping (2×10^{16} cm$^{-3}<N_d<1\times10^{17}$ cm^{-3}) and mobilities of 2500–3000 cm^2/V s at room temperature. We believe the high backgrounds are due to impurity incorporation from the trimethylarsenic, as has been reported by others.[3] Trimethylarsenic was selected on the basis of safety; it is known that arsine produces much higher purity films.

Our reactor design is shown in Fig. 1. Since layer switching is now done thermally, it is possible to use a simplified gas control system. The wafer sits on a thin (20 mil) graphite susceptor heated from the underside by a bank of high power tungsten halogen lamps, as in a rapid thermal annealer. Temperature is measured with a thermocouple inserted down a 2-mm-o.d. sealed quartz tube in contact with the susceptor. For initial calibration an additional thermocouple is welded to the sample[4] and the relationship between the wafer temperature and the inserted thermocouple is established. The graphite susceptor is used for temperature measurement only; we believe that supporting the sample on quartz pins alone and measuring temperature with an optical pyrometer would improve this technique by reducing thermal rise and fall times.

In rapid thermal MOCVD gas flows are initiated and stabilized while the wafer is cool. The growth of epitaxial layers is initiated by pulsing the lamps and bringing the wafer rapidly to growth temperature. At the end of each layer the lamps are shut off, the wafer cools rapidly toward room temperature, and the reaction is halted. The cooling rate is

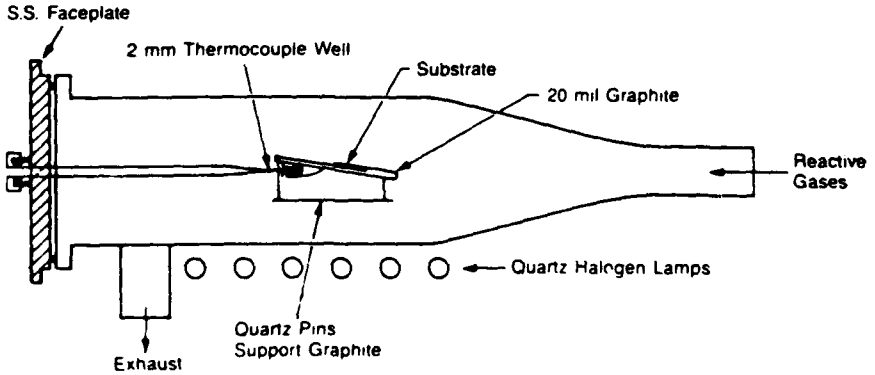

FIG. 1. Schematic drawing of the quartz reaction chamber used in our experiments. The wafer sits on a low thermal mass graphite susceptor and temperature is monitored by a thermocouple sheathed in a 2-mm-o.d. quartz tube.

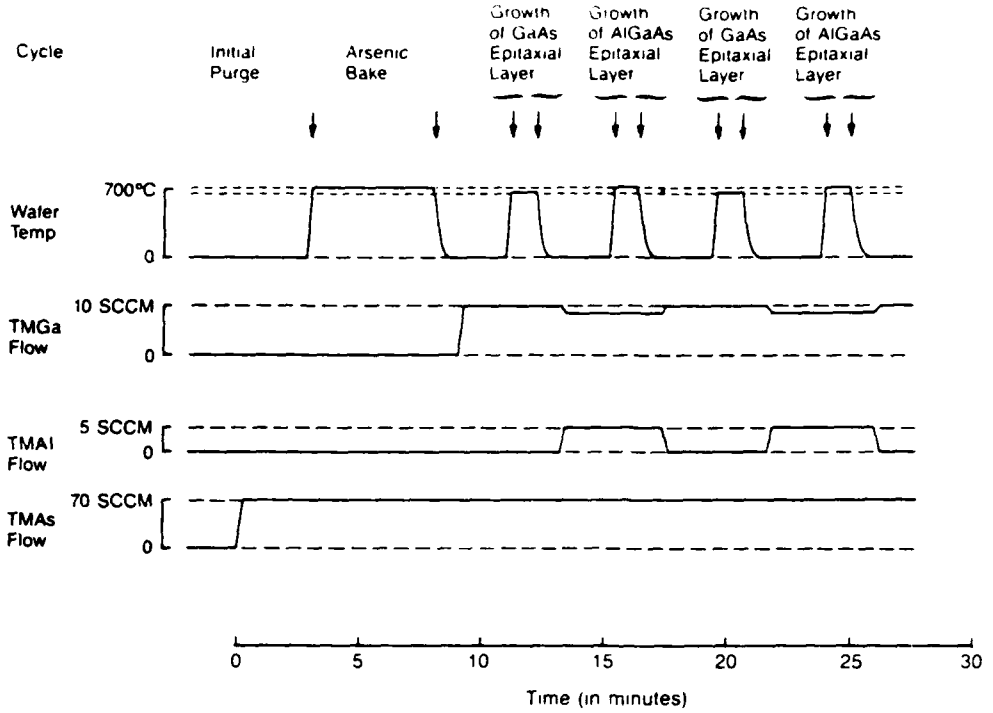

FIG. 2. LRP process timing diagram showing how layers are grown by pulsing the wafer temperature in the presence of the correct reactive gases.

enhanced by cooling the walls of the quartz reaction chamber with a high flow of compressed air, switched on at the termination of layer growth. Heat conducts rapidly away from the wafer through the hydrogen carrier gas. Rise and fall times are on the order of 10 s. Any desired structure may be grown by a sequence of these steps, as shown in Fig. 2 for a GaAs/$Al_xGa_{1-x}As$ multilayer structure. Note that the GaAs is grown at 670 °C and the AlGaAs at 720 °C. We found these temperatures gave the best mobility and surface morphology for single layers of each material.

One of our early concerns was that poor material would be grown during the cool down period, creating defects in the growth of subsequent layers. Test structures consisting of multiple layers of GaAs or alternating layers of GaAs/AlGaAs (3–11 layers, 500–2500 Å layer thickness) have been grown by a sequence of rapid thermal cycles. These structures have excellent surface morphology and electrical characteristics, equivalent to single layers grown by conventional MOCVD in our reactor. Such test structures have been analyzed by Rutherford backscattering and ion channeling, showing no evidence of crystal defects at the interfaces. Minimum yields are about 4.0%, the same as bare GaAs wafers. Rutherford backscattering detects only gross crystal defects; more sensitive tests of interface quality are in progress, including device fabrication and high resolution transmission electron microscopy.

An Auger depth profile of a GaAs/$Al_{0.12}Ga_{0.88}As$ multilayer structure grown by this technique is shown in Fig. 3. Layers are abrupt to within the resolution of Auger (50–60 Å). The total thickness of this structure is about 6000 Å. Because gases are completely purged between layers, we believe this technique is capable of atomically abrupt interfaces.

In conclusion, we have demonstrated rapid thermal MOCVD by growing multiple layers of high quality III-V compound semiconductors. These layers exhibit electrical characteristics and surface morphology equivalent to layers produced by traditional MOCVD in our reactor. The rapid thermal MOCVD technique promises abrupt interfaces and thin layers combined with high growth rates.

We would like to acknowledge the technical assistance of K. E. Williams and helpful discussions with D. Houng of Hewlett-Packard Laboratories, C. P. Kuo of Hewlett-Packard Optoelectronics Division, and H. Beneking of Aachen

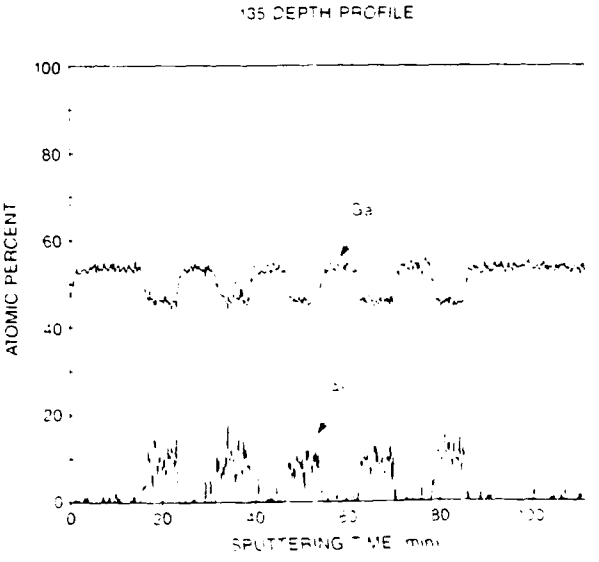

FIG. 3. Sputtering Auger profile for sample 135 showing a structure of alternating GaAs/$Al_xGa_{1-x}As$ layers. Total thickness is about [illegible] Å. Aluminum scaled by 2. Charles Evans and Associates, Redwood City, CA.

Technical Institute, Aachen, West Germany. We also acknowledge the support of J. Zavada and D. A. Reynolds at Defense Advanced Research Projects Agency (contracts DAAG29-85-K-0054 and DAAG29-85-K-237). S. Reynolds acknowledges the support of an Office of Naval Research fellowship.

[1] J. F. Gibbons, C. M. Gronet, and K. E. Williams, Appl. Phys. Lett. 47, 721 (1985).
[2] C. M. Gronet, J. C. Sturm, K. E. Williams, J. F. Gibbons, and S. D. Wilson, Appl. Phys. Lett. 48, 1012 (1986).
[3] C. A. Tromson, P. Gibart, R. Druilhe, Y. Monteil, J. Bouix, and B. El Jani, Rev. Phys. Appl. (France) 20, 569 (1985).
[4] J. L. Hoyt and J. F. Gibbons, Mater. Res. Soc. Symp. Proc. 52, 15 (1986).

Rapid thermal annealing of Si-implanted GaAs with trimethylarsenic overpressure

S. Reynolds, D. W. Vook, W. G. Opyd, and J. F. Gibbons
Stanford University Electronics Laboratories, McCullough 226, Stanford, California 94305

(Received 11 May 1987; accepted for publication 22 July 1987)

We have developed a novel rapid thermal processor to perform annealing of ion-implanted GaAs in a trimethylarsenic overpressure. This has allowed study of arsenic ambient annealing in a time/temperature regime not accessible with an arsine furnace. We have compared Si implant activation efficiency and surface degradation for arsenic ambient and proximity capped anneals. The arsenic ambient gives consistently higher activation efficiency with better surfaces.

The annealing of ion-implanted GaAs has received much study because of its practical importance for field-effect transistor fabrication.[1] Preferential As evaporation from the surface must be avoided. This is normally done either by providing an arsenic overpressure in a hot wall furnace, or by rapid thermal annealing (RTA) with a deposited encapsulated or proximity cap. For practical reasons, none of these methods is entirely satisfactory. Arsenic furnaces involve long thermal exposure and use large quantities of arsine. Deposited encapsulants (such as Si_3N_4 or SiO_2) stress the surface and tend to crack, causing localized increases in surface deterioration.[2]

We report rapid thermal annealing of GaAs with trimethylarsenic (TMAs) overpressure, which has advantages over the previous techniques. Thermal exposure can be minimized and arsenic overpressure need only be supplied for a short time. Surface morphology is better preserved when no encapsulant or proximity cap touches the GaAs surface. As ambient anneals have been studied for short times unobtainable in an arsine furnace, and As ambient RTA has been compared with the proximity capping method. We have also done preliminary experiments with nitride encapsulation. Proximity capping was used for comparison because it is a readily duplicated method. Results obtained with nitride caps are more dependent on the deposition conditions, so comparisons between laboratories are more difficult.

A schematic drawing of our annealer is shown in Fig. 1. The design is chosen to meet the problem of maintaining an arsenic overpressure in a cold wall reactor. A very thin (2 mil) molybdenum sheet, rolled into a semicylinder, slides inside a quartz tube and is open at the bottom toward the tungsten halogen lamps. It absorbs enough heat to prevent arsenic depletion near the wafer, reaching over 500 °C about 5 s after the lamps are switched on. Without it, arsenic condenses on the quartz walls and reduces the effective arsenic overpressure. The molybdenum sheet is, in effect, a rapid thermal wall. The samples are supported and heated indirectly by a thin (30 mil) graphite susceptor. A 1/64-in. stainless-steel sheathed thermocouple is inserted in the susceptor for closed loop temperature control. The tube is cooled with a high flow of compressed air, switched on at the end of the anneal cycle. Rise and fall times are on the order of 10 s.

Anneals were performed in 1 lpm of flowing H_2 gas, with or without TMAs. TMAs was transported in vapor form by passing H_2 through a bubbler held at -5 °C. A TMAs partial pressure of 2 Torr was found to be adequate to protect the surface up to 850 °C. For experiments involving higher temperatures, a pressure of 4 Torr was used. TMAs was selected because it was less toxic and easier to handle than arsine. In this application the additional methyl groups from TMAs do not appear to be much of a disadvantage. Our rapid thermal annealer is cleaner than an arsine furnace because TMAs only decomposes while the susceptor is hot. Since anneal times are so short, comparatively little arsenic dust is generated.

We first investigated the effect of annealing time on implant activation efficiency. We made Hall effect measurements in the van der Pauw configuration to determine the sheet carrier concentration, then divided this number by the implant dose. For temperatures ≥ 830 °C anneal time has little effect on activation, as shown in Fig. 2 for a 10^{13} cm^{-2}, 50 keV Si implant. A 10-s anneal is just as effective as a much longer one for implant activation. This suggests that most of the time a wafer spends in an arsine furnace may be unnecessary thermal exposure.

Activation efficiency as a function of temperature has been studied for a variety of Si implant doses, comparing TMAs ambients to Si proximity caps. Doses ranged from 10^{13} to 10^{15} cm^{-2}. In all cases the highest activation efficiency was obtained with TMAs overpressure. Results for a 10^{13} cm^{-2}, 50 keV implant are shown in Fig. 3. Optimum

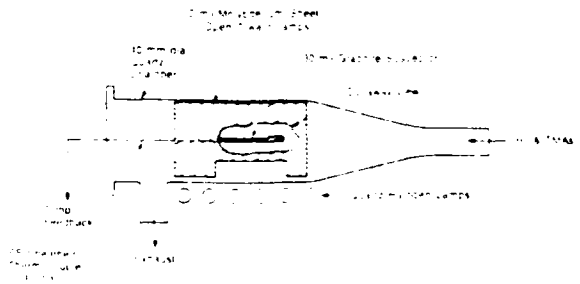

FIG. 1. Schematic drawing of the rapid thermal annealer used for trimethylarsenic overpressure annealing.

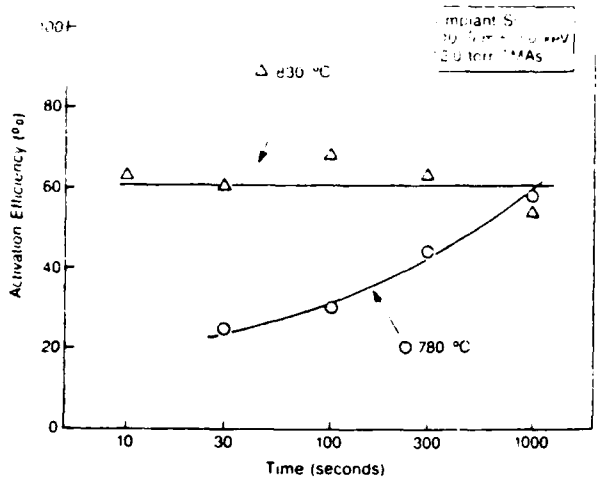

FIG. 2. Activation efficiency vs anneal time for TMAs ambient anneals.

annealing temperatures were 870 °C for the proximity cap and 900 °C for TMAs, yielding electron mobilities of 2600 cm^2/V s in both cases. The corresponding activations were 50–55% for the proximity cap and 60–65% for the TMAs. The improvement afforded by TMAs increases at higher annealing temperatures. Secondary ion mass spectroscopy (SIMS) depth profiling verified that no Si diffusion occurred for 10 s anneals at 900 °C, in TMAs or with Si proximity caps.

Some of our implant samples were encapsulated with Si_3N_4 by a low-pressure plasma enhanced process at 200 °C. The maximum activation efficiencies were about two-thirds as high as obtained for similar samples annealed in TMAs. Visible blistering of the nitride was observed for 10 s anneals at 900 °C and above. After removing the nitride, damage to the GaAs surface of these samples was observed under our Nomarski microscope (unannealed samples with the nitride removed had no damage). Surface damage was occasionally observed even for those lower temperature samples which did not blister. Other workers have obtained good results with nitride encapsulation, so our results with it should not be taken as conclusive.[3,4] Nitride encapsulation seems to be a process which must be optimized by each laboratory using it.

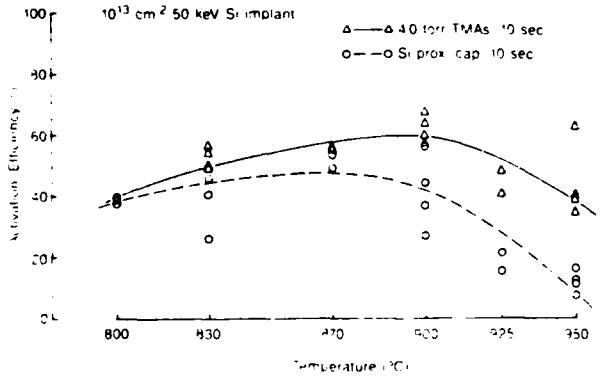

FIG. 3. Activation efficiency vs anneal temperature for 10 s anneals, comparing TMAs ambients to Si proximity caps.

sure alone remained featureless for all anneal conditions. The surface protected by a Si proximity cap alone without TMAs began showing signs of localized pitting for 10 s anneals at 925 °C. The surface degradation was visible by eye for 10 s anneals at 950 °C. The silicon proximity caps were inspected after each anneal and replaced if there was any sign of discoloration.

In our first experiments, GaAs wafers were used as proximity caps. We unexpectedly discovered that GaAs proximity caps are much less effective than Si caps at protecting the surface. Despite the use of a new GaAs cap for each anneal, the proximity caps themselves seem to decompose and promote further decomposition of the underlying wafer. With GaAs caps, surface decomposition visible to the eye begins as low as 850 °C for a 10-s anneal.

TMAs overpressure is thus much more effective than proximity capping at preventing gross surface decomposition. Auger sputter profiling was used to make a qualitative comparison of surface composition at lower temperatures, where both As overpressure and proximity capping yielded featureless surfaces under the microscope. The differences revealed by Auger were smaller than expected (for 830 °C anneals). Figure 4 shows a set of Auger profiles for a sample annealed in TMAs (10 s at 830 °C), then exposed to room air. The most notable feature is the oxygen signal extending about 120 Å into the sample. A decrease in the As signal extends to about the same depth. Samples annealed with a proximity cap are very similar, but appear to develop a slightly thicker native oxide. To quantitatively compare the extent of oxidation, we integrated the oxygen and arsenic signals to determine the relative O gain and As loss. The results are shown in Table I. While both anneal conditions generate some surface deterioration, TMAs annealed surfaces are better.

In summary, we have designed a TMAs ambient rapid thermal annealer which maintains an As overpressure in a

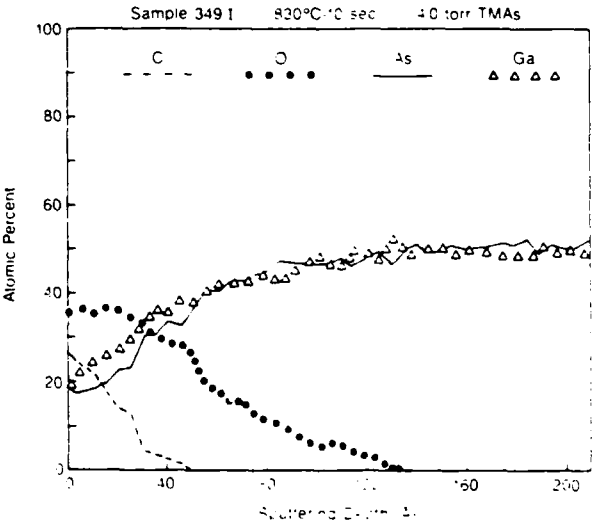

FIG. 4. Auger sputtering profiles (Ga, As, C, O) for a sample annealed in TMAs (10 s at 830 °C) and then exposed to air. Unannealed samples also have the surface C peak (Charles Evans and Associates, Redwood City, CA).

TABLE I. Comparison of the oxygen gain and As loss for samples annealed under various conditions (and then exposed to room air), obtained by integrating the Auger oxygen and arsenic signals.

Sample	Annealing conditions	O gained in surface oxide (10^{15} atoms/cm^2)	As lost from bulk to ambient or into surface oxide (10^{15} atoms/cm^2)
I	as-implanted unannealed	5.1	2.5
349I	10 s @ 830 °C TMAs	12.1	7.8
343I	10 s @ 830°C Si prox. cap	15.7	8.7

nominally cold wall reactor. These are the first RTA experiments using a controlled As overpressure similar to an arsine furnace. We have observed that short anneals in As appear to be as effective as long ones for activating implants, so that the added thermal exposure of an arsine furnace may be unnecessary. Rapid As ambient anneals give higher activation of Si implants and less surface decomposition than proximity capping, as expected.

We would like to acknowledge the support of J. Zavada at the Army Research Office and D. A. Reynolds at the Defense Advanced Research Projects Agency. S. Reynolds acknowledges the support of an Office of Naval Research Fellowship. We thank S. Bui of Avantek for technical assistance.

[1] R. E. Williams, *Gallium Arsenide Processing Techniques* (Artech, Dedham, MA, 1984), p. 47.
[2] G. J. Valco and V. J. Kapoor, J. Electrochem. Soc. **134**, 569 (1987).
[3] N. J. Barrett, J. D. Grange, B. J. Sealy, and K. G. Stephens, J. Appl. Phys. **57**, 5470 (1985).
[4] T. E. Haynes, W. K. Chu, and S. T. Picraux, Appl. Phys. Lett. **50**, 1071 (1987).

Paper #1

Open-tube Zn diffusion in GaAs using diethylzinc and trimethylarsenic: Experiment and model

S. Reynolds, D. W. Vook, and J. F. Gibbons
Stanford University Electronics Laboratories, McCullough 226, Stanford, California 94305

(Received 30 July 1987; accepted for publication 27 October 1987)

We have characterized the diffusion of Zn into GaAs from the organometallic sources diethylzinc and trimethylarsenic. This method produces surface hole concentrations in excess of 10^{20} cm^{-3} with good control of junction depths as shallow as 0.1 μm. Smooth surface morphology is retained. The profile shape is much more complex than the accepted interstitial-substitutional Zn-diffusion model would predict. To explain the observed profiles, a new model for Zn diffusion is proposed and implemented in a computer simulation.

I. INTRODUCTION

Zn diffusion in GaAs is an important processing step in the fabrication of diodes, junction field-effect transistors (JFETs), and bipolar transistors.[1] Unfortunately, control over the diffusion process has often been difficult and can limit device performance. Widely varying results with Zn diffusion have been reported. An understanding of the physical mechanisms of the diffusion process may allow it to be brought under better control.

Vapor phase diffusions using a diethylzinc (DEZn) source were reported in a paper by Dohsen *et al.*[2] These authors fabricated GaAs JFETs by localized diffusion through a patterned nitride (Si_3N_4) mask. We employed this vapor phase diffusion method to perform blanket diffusions for the fabrication of p^+-i-n diodes. In doing so, we observed that the junction depth and profile shape are a complicated function of the diffusion conditions. We report our experimental results using this method, and we propose a new model to explain the complex profile shapes.

It is widely accepted that Zn diffuses in GaAs by an interstitial-substitutional mechanism, similar to that proposed by Frank and Turnbull[3] for Cu in Ge. In this model, a small fraction of the total dissolved Zn is present interstitially. This interstitial Zn diffuses rapidly and dominates the diffusion process. This model predicts an abrupt concentration-dependent diffusion profile where the effective diffusion coefficient is proportional to the square of the total Zn concentration.[4] This model works well in the high-concentration surface region of our Zn profiles, but it does not predict the complex double profiles that we and others[5] have observed. Our model is a modification of the interstitial-substitutional mechanism.

II. EXPERIMENTAL PROCEDURE

Diffusions were carried out in a hot-wall quartz reaction chamber (40 mm diam) at atmospheric pressure, with 1 l/min of H_2 carrier gas flow. Trimethylarsenic (TMAs) and DEZn were transported in vapor form by flowing H_2 through bubblers held at constant temperature. The TMAs and DEZn partial pressures (p_{TMAs} and p_{DEZn}) were varied over a range from 0.1 to 3.0 Torr. TMAs was used to prevent GaAs surface decomposition at elevated temperatures.

GaAs wafers were undoped (100) Czochralski material polished on one side, obtained from Morgan semiconductor. The dislocation densities, as specified by the manufacturer, ranged from 2×10^4 to 4.3×10^4 cm^{-2}. Samples were degreased with organic solvents prior to loading. When we first observed the complex profile shape, we wondered if it was due to residual surface damage from the manufacturer. One set of samples was degreased and etched for 5 min in 5:1:1 H_2SO_4:H_2O_2:H_2O prior to loading. By simultaneously processing another set of samples which were degreased only, we verified that etching the wafers had no effect on diffusion rates or profile shape. To be consistent, all samples included in the data presented here were degreased only.

Samples were loaded into the reaction chamber on a graphite susceptor. The chamber was evacuated, then backfilled with H_2 and purged. TMAs flow was started and the sample was ramped to the diffusion temperature in 3 min. After 1 min at the diffusion temperature the DEZn was switched on. At the end of the diffusion time the DEZn was switched off, the chamber was purged for 1 min, then cooled. When the susceptor reached 500 °C the TMAs was switched off. Total cooling time to below 100 °C was less than 5 min.

Controlling the diffusion by switching the DEZn flow was found to be the most satisfactory method. If the susceptor is cooled rapidly with DEZn flowing, elemental Zn condenses on the wafer. Thus, temperature switching is ineffective. By switching on the DEZn flow for a period of several tens of seconds, diffusions could be well controlled to depths as shallow as 0.1 μm. Well-controlled shallower diffusions might be obtained by increasing the H_2 flow, thus purging the chamber more quickly. The only disadvantage of switching the DEZn flow to control junction depth is a small amount of out-diffusion near the GaAs surface, which can be seen in Fig. 1. Tuck and Houghton[6] showed that when Zn-doped GaAs is annealed without a Zn source, very little further movement of the Zn profile occurs. Thus, Zn diffuses rapidly only when it is being incorporated at the surface. Our results, discussed in Sec. III confirm this observation. This behavior is important in developing a Zn-diffusion model.

Samples diffused over the temperature range from 650–750 °C had smooth, specular, and generally featureless surfaces when examined under our Normarski microscope. Samples diffused much above 750 °C begin to show signs of surface roughening. Samples diffused below 625 °C show

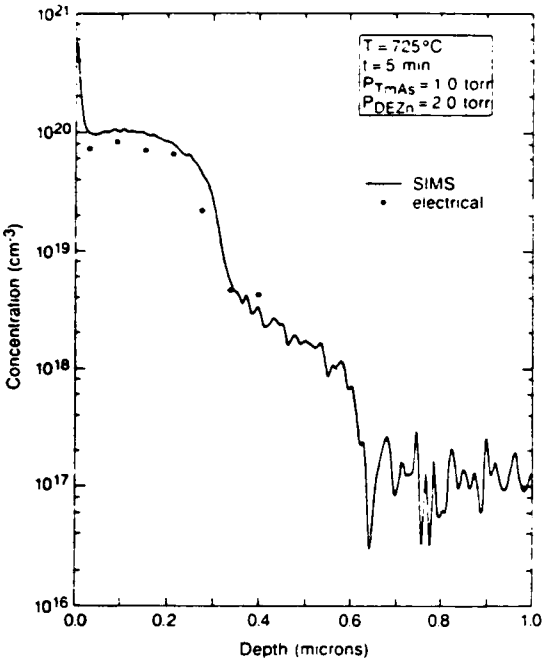

FIG. 1. Electrical and SIMS profiles for a 5-min diffusion at 725 °C. The surface peak is a SIMS artifact, but the dip immediately behind it is probably a small amount of out-diffusion from the 1-min final purge (see discussion in Sec. II).

areas of what we believe to be metallic Zn condensation if high DEZn flows are used.

The walls of the reaction chamber receive fairly heavy deposition of As, Zn, and Zn_xAs_y compounds, comparable in degree to a GaAs metalorganic chemical vapor deposition (MOCVD) reactor. Since this is a hot-wall reactor, these deposits can have an unpredictable effect on subsequent diffusions at a different temperature or DEZn flow. Therefore, the reaction chamber was baked out at a high temperature (>900 °C) with flowing TMAs between each diffusion to remove volatile Zn compounds (it was removed and chemically cleaned every 3–4 runs). With the reaction chamber baked out or chemically cleaned between runs, we were able to reproduce junction depths to within $\pm$ 15%. We verified that samples annealed with no DEZn flow (TMAs only) after the chamber had been baked out showed no measureable conductivity. Note that it would be difficult to carry out this diffusion method in a cold-wall reactor. Zn and As would diffuse from the hot zone near the susceptor and deposit on the cold walls, making it difficult to maintain the required Zn and As partial pressures.

Zn concentration profiles in the diffused samples were measured by secondary ion mass spectrometry (SIMS).[7] Electrical measurements were made by the differential van der Pauw technique. In this method, sheet resistance and Hall voltage are measured at the GaAs surface. Carrier concentrations are obtained by successively etching away thin GaAs layers and then remeasuring sheet resistance and Hall voltage. We have analyzed more than 40 profiles by either SIMS, electrical measurements, or both

III. EXPERIMENTAL RESULTS

Figure 1 shows electrical and chemical profiles for a 5-min diffusion at 725 °C. The most notable feature is the long tail extending beyond the high-concentration surface region. Electrical measurements imply that virtually all of the Zn is electrically active, probably even in the tail region. Electrical measurements do not extend to the same depth as SIMS measurements because the contacts on a van der Pauw sample generally fail before the conductive layer is completely removed.

Figure 2 shows SIMS profiles for a set of five diffusions carried out at temperatures from 650–750 °C. The plots have a normalized depth scale to show the change in profile shape. To do this, we defined x_j as the point on each curve where the Zn concentration equals 10^{19} cm^{-3}, then divided the depth scale for each curve by this x_j. The relative size of the tail region grows larger at higher diffusion temperatures. The 650 °C diffusion is the most desirable from a device processing standpoint, since it has the highest surface concentration and a small tail region. Hole concentration for the 650 °C diffusion was 1.3×10^{20} cm^{-3}.

Figure 3 is a set of SIMS profiles for diffusions carried out at 700 °C for various times from 1–10 min. Figure 4 shows the progression of three points on each profile plotted versus the square root of time. This figure suggests that the entire Zn-diffusion profile scales with the square root of diffusion time, so that the general profile shape does not change. This is further suggested by Fig. 5, in which the four

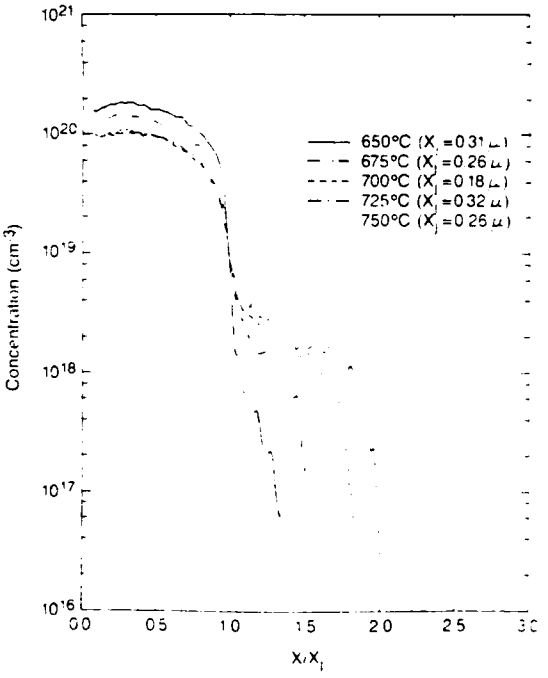

FIG. 2. SIMS profiles for a set of five diffusions carried out over a temperature range from 650–750 °C (p_{TMAs} = 1.0 Torr, p_{DEZn} = 2.0 Torr). The plots have a normalized depth scale to show the change in profile shape. The (x/x_j) = 1 point on this scale is the place where the Zn concentration is 10^{19} cm^{-3}; the actual depth to which this corresponds is shown in parentheses.

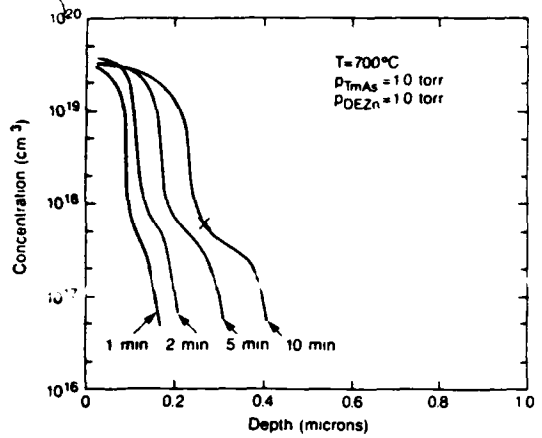

FIG. 3. SIMS profiles for a set of four diffusions carried out at 700 °C for times from 1–10 min.

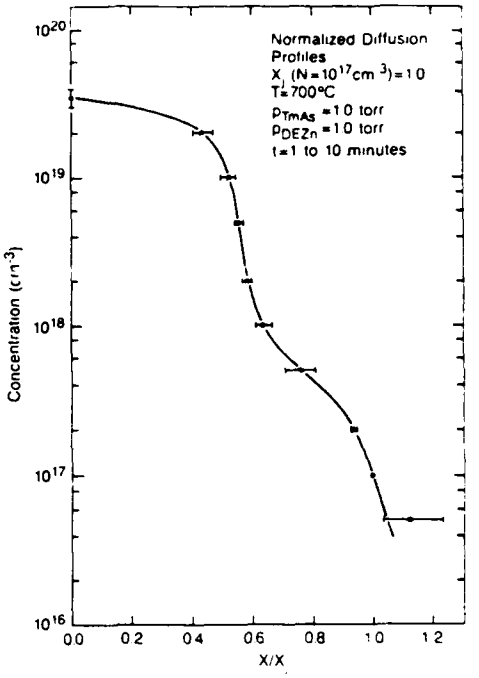

FIG. 5. The four SIMS profiles from Fig. 3 are shown plotted on a normalized depth scale. The depth at which the Zn concentration of each profile falls to 10^{17} cm^{-3} is set equal to 1.0. The error bars show the maximum deviation of any profile from the average of the four The change in profile shape with time appears to be very small.

profiles of Fig. 3 are replotted on a normalized depth scale. The error bars in Fig. 5 show the maximum deviation of any profile from the average of the four. Within our experimental error, the shape of the diffusion profile does not change with time. Dohsen *et al.*[2] show a similar result to that in Fig. 4. Figures 3–5 also indicate that relatively little movement of the Zn profile occurs during the 1-min purge after the DEZn flow is switched off. If significant movement did occur, one would expect the relative change to be much greater in a 1-min diffusion than a 10-min one.

For the purpose of comparing the various diffusion profiles, it is convenient to define a "kink level" where the two different portions (the surface region and the tail) of each profile meet. Each profile has a small section in which it is concave up; the kink level is defined as the point where the second derivative is at a maximum. The "x" in Fig. 3 is an example of the kink level. Figures 6 and 7 show the kink level of several profiles plotted against diffusion time and temperature. Kink level rises with temperature and is approximately independent of time. Figure 7 also shows the variation of surface concentration with temperature.

We have studied the effect of DEZn and TMAs partial pressures on the diffusion profiles. For a range of p_{DEZn} from 0.2–2.0 Torr, Zn surface concentration increases linearly with p_{DEZn}. If we ignore the tail region of the profiles and apply the interstitial-substitutional (I-S) model to surface region ($C \gtrsim 10^{19}$ cm^{-3}), we can extract a surface diffusivity according to the equations of Weisberg and Blanc[4]:

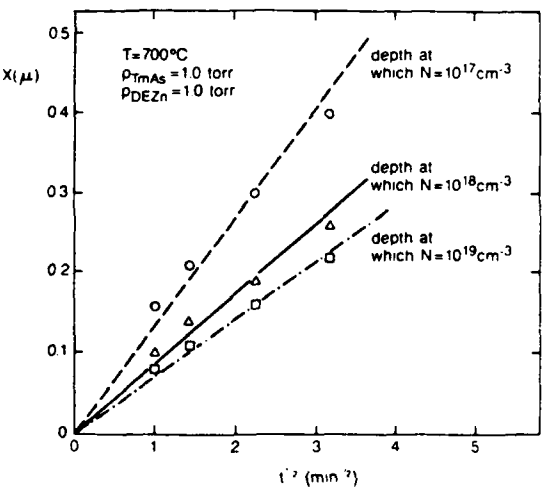

FIG. 4. The junction depth of various Zn concentrations ($N = 10^{17}$; $N = 10^{18}$, and $N = 10^{19}$ cm^{-3}) for the SIMS profiles shown in Fig. 3, plotted vs the square root of diffusion time.

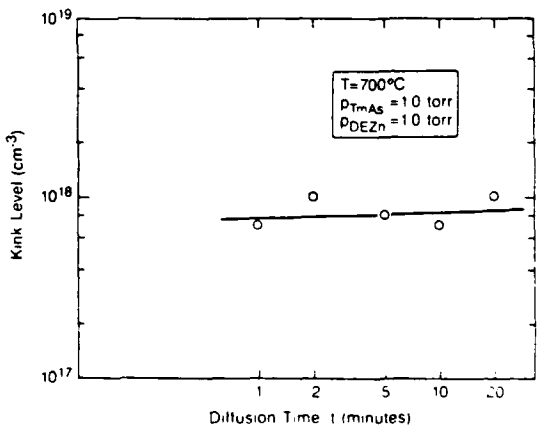

FIG. 6. Kink level as a function of diffusion time. Kink level is defined as the point where the two different portions (the surface region and the tail) of each profile meet. An example is the "x" in Fig. 3.

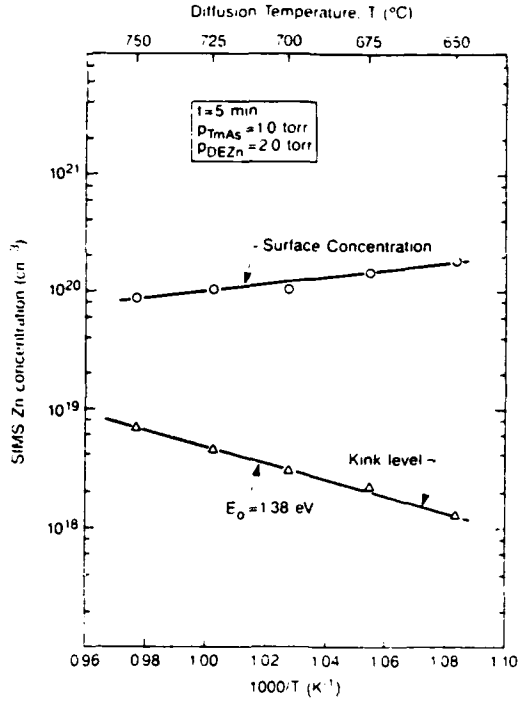

FIG. 7. Kink level and surface concentration as a function of inverse diffusion temperature.

$$D_{sur} = (x_j/1.092)^2(1/t),$$
$$D = D_{sur}(C/C_{sur})^2.$$

Figure 8 plots this extracted surface diffusivity against the DEZn partial pressure. The slope of the straight line is 2, indicating a good fit to the interstitial-substitutional model in the surface region. TMAs partial pressure has only a small effect on the profiles over a range from 0.2–3.0 Torr. At 650 °C, D_{sur} decreases as approximately the fourth root of p_{TMAs} as the I-S model predicts.

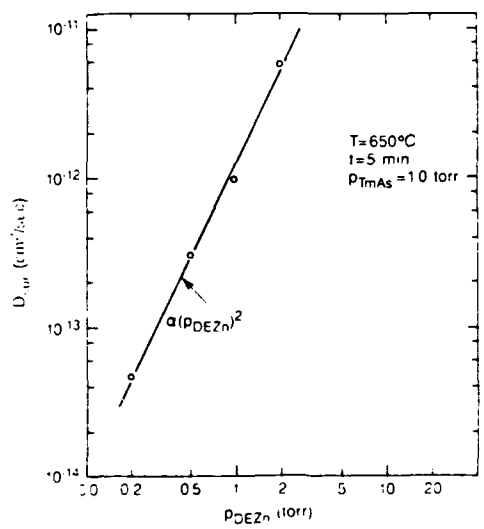

FIG. 8. Surface diffusivity (D_{sur}) plotted against DEZn partial pressure. Surface diffusivity is defined by the equation $D_{sur} = (x_j/1.092)^2(1/t)$. To extract D_{sur}, x_j is taken as the point where $C = [Zn] = 10^{19}$ cm^{-3}.

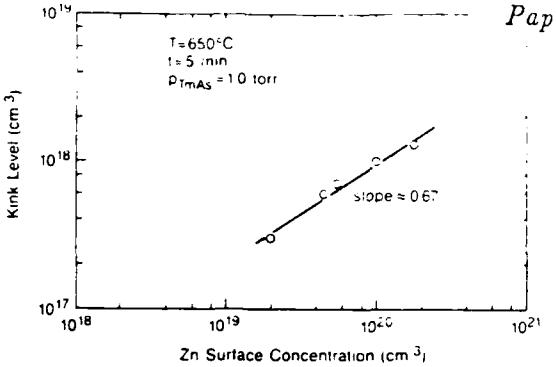

FIG. 9. Kink level plotted as a function of Zn surface concentration, C_{sur} (C_{sur} was adjusted via p_{DEZn}).

Figure 9 shows the variation of kink level with Zn surface concentration (C_{sur}). C_{sur} varied by adjusting the DEZn partial pressure. The kink level varies as approximately the 0.67 power of C_{sur}, although the power dependence could actually be from 0.5 to 1.0 if experimental error is considered.

IV. MODEL

Double profile or kinked Zn diffusions have been observed by Tuck and Kadhim.[5] Their data also indicate a change in profile shape with diffusion time, which they attribute to the gallium vacancy concentration falling below its thermal equilibrium value. Similar data and a more general model are discussed in a paper by Ting and Pearson.[8] Gösele and Morehead[9] propose a slightly different mechanism to explain the data of Tuck. They suggest that the dominant defect in GaAs may be interstitial gallium (I_{Ga}) and that the kink occurs because I_{Ga} is present in excess of its thermal equilibrium value both near the diffusion front and in the tail region. These models are all quite plausible, and the nonequilibrium they describe probably does occur under certain conditions. However, the concentration dependence of the diffusion coefficients they predict does not exactly match our data (or Tuck's). We propose that the double profile is caused by the existence of two different species of diffusing Zn (in addition to substitutional Zn) which dominate in different locations according to the position of the Fermi level.

We begin our analysis by determining the effective Zn diffusion coefficient as a function of concentration from the SIMS profiles. Tuck and Kadhim[5] have pointed out that the standard Boltzmann–Matano analysis[10] is not valid for a profile shape which changes with time. Since our data do not indicate the time dependence that Tuck observed, we have applied the Boltzmann–Matano method, but it is probably best to regard the result as an approximation. Our data do not prove that there is no time dependence, only that it is very small under our experimental conditions.

Figure 10 gives the result of our Boltzmann–Matano analysis. In the surface region we have $D_{Zn} \propto C^2$ as predicted by the I-S model. There is a transition region between about 2×10^{18} and 2×10^{19} cm^{-3} in which $D_{Zn} \propto C^{-2}$. The tail re-

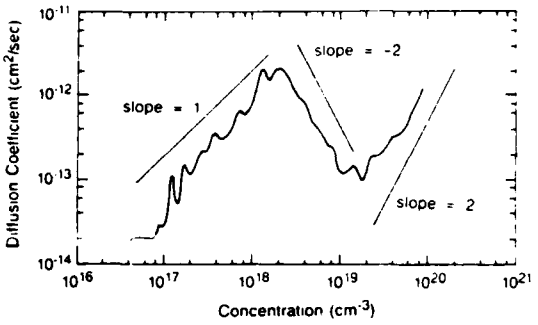

FIG. 10. Effective Zn-diffusion coefficient as a function of concentration for the SIMS profile in Fig. 1, obtained by Boltzmann–Matano analysis.

gion is noisy and it is difficult to determine whether we have $D_{\text{eff}} \propto C$ or $D_{\text{eff}} \propto C^2$, although for the particular data in Fig. 10, $D_{\text{eff}} \propto C$ appears to give a better fit. The concentration dependence can also be determined by fitting calculated diffusion profiles to the SIMS data. The profiles which result from assuming either $D_{\text{eff}} \propto C^2$ or $D_{\text{eff}} \propto C$ can be calculated by the method of Weisberg and Blanc.[4] Figure 11 shows the SIMS data of Fig. 1 fit with a $D_{\text{eff}} \propto C^2$ profile in the surface region and a $D_{\text{eff}} \propto C$ profile in the tail. For all of our SIMS data, assuming a $D_{\text{eff}} \propto C$ profile gives a much better fit to the tail region than $D_{\text{eff}} \propto C^2$. $D_{\text{eff}} \propto C$ also appears to give a better fit to the tail region of Tuck's data, shown in Fig. 4 of Tuck and Kadhim.[5] Neither Tuck's nor Gösele's model for Zn diffusion predicts this change in concentration dependence.

In the I-S model, substitutional Zn occupies the Ga sub-

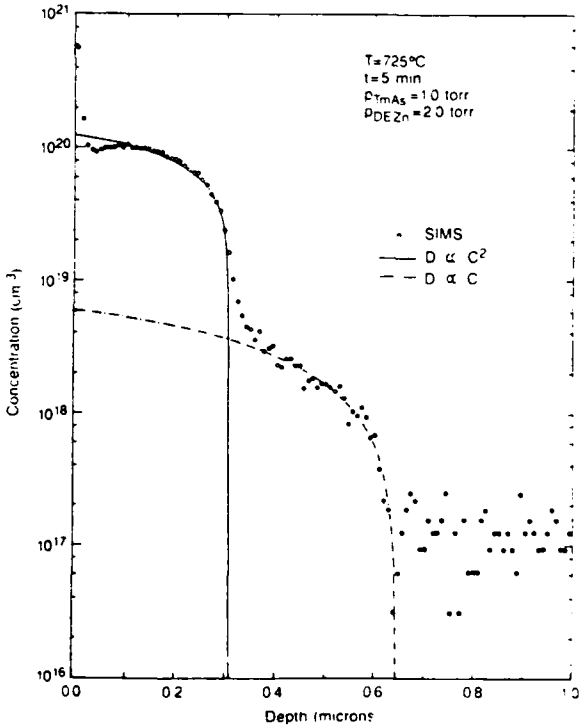

FIG. 11. Calculated diffusion profiles have been fit to the SIMS data of Fig. 1. Assuming a $D_{\text{eff}} \propto C^2$ gives a good fit to the surface region; $D_{\text{eff}} \propto C$ fits better in the tail.

lattice as a shallow acceptor (Zn_i^-), while interstitial Zn is considered to be a singly or doubly ionized donor (Zn_i^+ or Zn_i^{++}). The solubility of Zn_i^- is much greater than that of interstitial Zn, while interstitial Zn has a diffusion coefficient several orders of magnitude greater. Interstitial Zn enters the lattice at the surface, moves rapidly to the diffusion front, and becomes substitutional according to either

$$Zn_i^- + V_{Ga}^- \rightleftharpoons Zn_s^- + 2h^+$$

or

$$Zn_i^{++} + V_{Ga}^- \rightleftharpoons Zn_s^- + 2h^+,$$

where h^+ are holes. Both of these reactions yield $D_{\text{eff}} \propto C^2$. Precisely which reaction occurs is not agreed upon. Seemingly contradictory evidence (from isoconcentration studies) exists for both Zn_i^+ and Zn_i^{++}.[11,12]

Figure 11 tends to suggest that two different diffusing species or mechanisms are involved in the diffusion. We propose that Zn can exist as either a singly ionized interstitial (Zn_i^-) or a doubly ionized interstitial (Zn_i^{++}), in addition to being a substitutional acceptor. Our model assumes that Zn_i^{--} is a deep donor level, within a few tenths of an eV from the valence-band edge. Zn_i^+ would also be a deep donor, but near the center of the band gap. We make this choice of donor level based on a study of Zn diffusion in heavily n-type GaAs by Wang.[13] Wang observed only substitutional Zn diffusion and concluded that Zn_i^- does not exist in n-type material. This places the Zn_i^- donor level at least a few tenths of an eV from the conduction-band edge, and probably deeper. The energy difference between Zn_i^+ and Zn_i^{++} can be estimated by the method of Harrison,[14] taking the difference between the first and second vacuum ionization potentials for Zn and dividing by the dielectric constant for GaAs:

$$\Delta E \simeq (E_2 - E_1)/\epsilon_{\text{GaAs}} = 0.65 \text{ eV}.$$

These donor levels are illustrated in the band diagram of Fig. 12.

The Zn_i^{--} would be formed at the surface and dominate the diffusion process in the heavily doped surface region. In less heavily p-type regions near the diffusion front, the Fermi level would move away from the valence-band edge. The more mobile Zn_i^+ would then be favored, giving rise to the diffusion tail and yielding a $D_{\text{eff}} \propto C$ dependence. This is summarized in the following reactions. We assume that interstitial Ga is the dominant defect, after Gösele.[9]

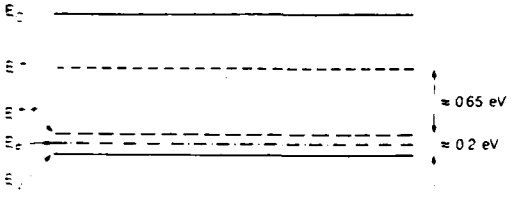

FIG. 12. GaAs band diagram, showing the position of the two donor levels assumed in the model. The E^{--} level for Zn_i^{--} is chosen to be about 0.2 eV from the valence-band edge as the best fit to our data. The E^+ level for Zn_i^+ is estimated to lie about 0.65 eV higher in energy, based on relative ionization potential.

These reactions would also work if we assumed V_{Ga}^{-} to be the relevant defect:

$$Zn_i^{+\,+} \rightarrow Zn_s^{-} + I_{Ga}^{+} + 2h^{+}, \quad (1a)$$

$$Zn_i^{+\,+} \rightarrow Zn_i^{+} + h^{+}, \quad (2a)$$

$$Zn_i^{+} \rightarrow Zn_s^{-} + I_{Ga}^{+} + h^{+}. \quad (3a)$$

Note that $Zn_i^{+\,+}$ must have a smaller diffusion coefficient than Zn_i^{+} in order for the model to work. This is physically plausible if the main barrier to interstitial motion is electrostatic. Although $Zn_i^{+\,+}$ has a smaller radius than Zn_i^{+}, they are probably both small compared to gaps in the GaAs lattice. There is the possibility that doubly ionized Zn forms some sort of charged complex with Ga or As atoms on the GaAs lattice, or with a point defect. The notion of a $(Zn_i - Ga)^{+\,+}$ or $(Zn_i - As)^{+\,+}$ complex is one way to conceptualize an electrostatic barrier to interstitial motion. Our model does not require the existence of any such complex, but only that the doubly ionized Zn diffuse more slowly than Zn_i^{+}.

The concentration of I_{Ga} is assumed to be everywhere equal to its equilibrium value. The following equations then hold if reactions (1a)–(3a) are in equilibrium:

$$C_{ii} = k_1 C_s^3, \quad (1b)$$

$$C_{ii} = k_2 C_s C_i, \quad (2b)$$

$$C_i = k_3 C_s^2, \quad (3b)$$

where $C_{ii} = [Zn_i^{+\,+}]$, $C_s = [Zn_s^{-}]$, and $C_i = [Zn_i^{+}]$. The parameters k_1 through k_3 are equilibrium constants. The observation that Zn diffuses rapidly only when it is being incorporated at the surface implies that reactions (1a)–(3a) go predominantly in one direction, as indicated by the large arrows. This is intuitively plausible because, in each case, going in the opposite direction would appear to require a higher activation energy. For instance, Zn interstitials might be readily formed at the surface because of unsatisfied bonds and a large excess of Zn. Once in the lattice, formation of $Zn_i^{+\,+}$ or Zn_i^{+} from Zn_s^{-} would require breaking bonds to the neighboring Ga and As atoms and leave a vacancy.

Under these conditions, our computer simulation is necessarily an approximation to the behavior of reactions (1a)–(3a). Our approximation is that the deviations of C_{ii} or C_i above the equilibrium concentrations predicted by (1b)–(3b) are corrected immediately via reactions (1a)–(3a). Deviations below the equilibrium value are allowed to persist (although they are corrected by diffusion). We solve the following equations for simultaneous diffusion and chemical reaction:

$$\frac{\partial C_{ii}}{\partial t} = D_{ii}\frac{\partial^2 C_{ii}}{\partial x^2} - \frac{\partial S_1}{\partial t} - \frac{\partial S_2}{\partial t}, \quad (4)$$

$$\frac{\partial C_i}{\partial t} = D_i\frac{\partial^2 C_i}{\partial x^2} + \frac{\partial S_2}{\partial t} - \frac{\partial S_3}{\partial t}, \quad (5)$$

$$\frac{\partial C_s}{\partial t} = \frac{\partial S_1}{\partial t} + \frac{\partial S_3}{\partial t}. \quad (6)$$

D_{ii} and D_i are the diffusion coefficients for doubly and singly ionized Zn interstitials. $(\partial S_1/\partial t)$ is the rate at which $Zn_i^{+\,+}$ become Zn_s^{-} according to reaction (1a). $\partial S_2/\partial t$ is the rate at

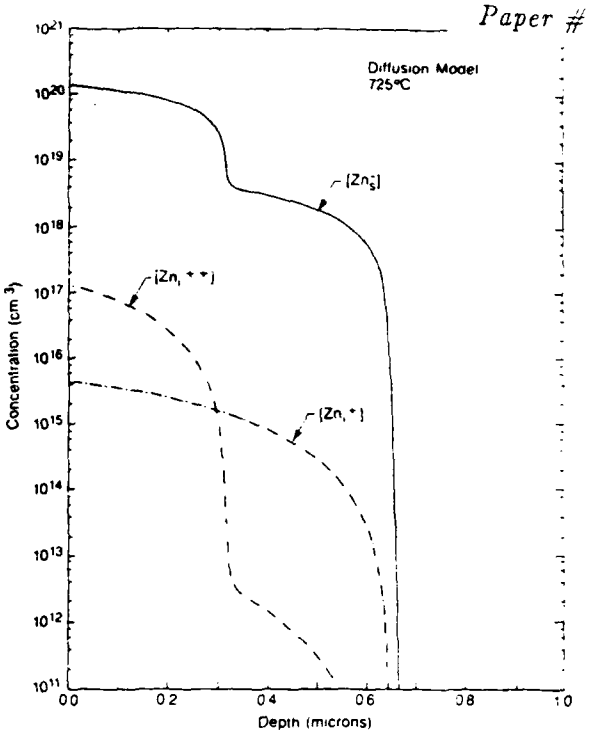

FIG. 13. Results of a computer simulation for a 5-min diffusion at 725 °C, showing the concentrations of Zn_s^{-}, $Zn_i^{+\,+}$, and Zn_i^{+}. Note that the total concentration of mobile Zn, which is assumed in the model to be much less than $[Zn_s^{-}]$, is arbitrarily taken to be 10^{-3} of the total Zn present at the surface.

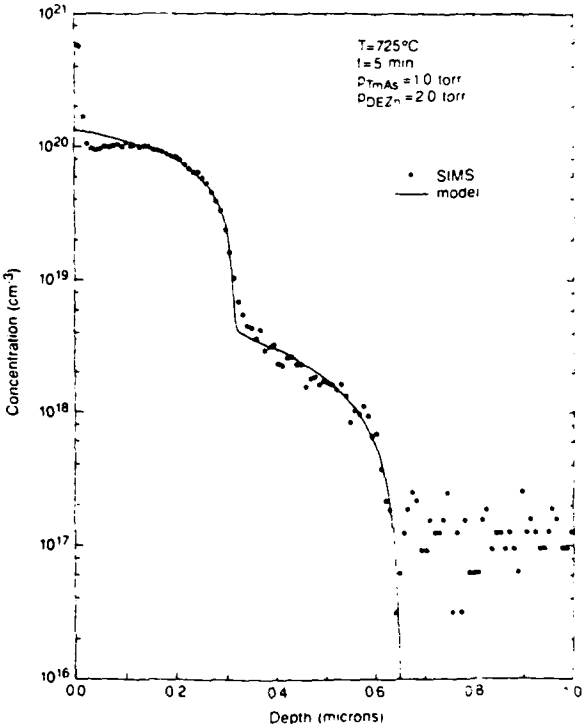

FIG. 14. SIMS data and a fitted computer simulation for a 5-min diffusion at 725 °C.

TABLE I. The model parameters used to fit our experimental data of Fig. 2.

Model parameter	Units	Temperature (°C)				
		650	675	700	725	750
C_{sur}	cm^{-3}	2.4×10^{20}	1.8×10^{20}	1.3×10^{20}	1.3×10^{20}	1.2×10^{20}
$D_{\parallel}$	cm^2/s	1.2×10^{-12}	0.8×10^{-12}	0.4×10^{-12}	1.2×10^{-12}	0.7×10^{-12}
D_i	cm^2/s	3.0×10^{-12}	3.0×10^{-12}	1.5×10^{-12}	5.0×10^{-12}	6.0×10^{-12}
$(k_2)^{-1}$	cm^{-3}	1.1×10^{18}	1.9×10^{18}	3.0×10^{18}	4.5×10^{18}	7.0×10^{18}
$k_3(k_1C_{sur})^{-1}$	no unit	20	17	15	12	9

which $Zn_i^{+\,+}$ become Zn_i^{+} according to reaction (2a). Finally, $\partial S_3/\partial t$ is the rate at which Zn_i^{+} become Zn_s^{-} via reaction (3a).

Equations (4)–(6) are solved by a finite difference algorithm, selecting small values for Δt and Δx. For each small time step Δt, the mobile species are allowed to diffuse according to

$$\Delta C_{\parallel}(x_n) = \Delta t\left(D_{\parallel}\frac{\partial^2 C_{\parallel}(x_n)}{\partial x^2}\right),$$

$$\Delta C_i(x_n) = \Delta t\left(D_i\frac{\partial^2 C_i(x_n)}{\partial x^2}\right).$$

Next, reaction (2a) is assumed to bring $C_{\parallel}(x_n)$ and $C_i(x_n)$ into equilibrium. $\Delta S_2(x_n)$ is obtained by calculating the expected equilibrium value for $C_{\parallel}^{eq}(x_n)$ from Eq. (2b), then taking the difference $\Delta S_2(x_n) = C_{\parallel}(x_n) - C_{\parallel}^{eq}(x_n)$. ΔS_2 is constrained to be ≥ 0, since we are allowing reactions (1a)–(3a) to proceed only in one direction. $C_{\parallel}(x_n)$ and $C_i(x_n)$ are adjusted using ΔS_2. Next, reactions (1a) and (3a) are assumed to bring $C_{\parallel}(x_n)$ and $C_i(x_n)$ each into equilibrium with $C_s(x_n)$. $\Delta S_1(x_n)$ and $\Delta S_3(x_n)$ are obtained as $\Delta S_2(x_n)$ was before. Finally, $C_{\parallel}(x_n)$, $C_i(x_n)$, and $C_s(x_n)$ are updated and t is incremented by Δt.

To obtain initial conditions, reactions (1a) and (2a) are assumed to be in equilibrium exactly at the GaAs surface. The Zn surface concentration $C_s(x=0) \equiv C_{sur}$ is known. Choosing k_2 fixes $C_{\parallel}(x=0)$ and $C_i(x=0)$ within an arbitrary constant. The other variable parameters are k_3, $D_{\parallel}$, and D_i (for a total of four at each temperature). Figure 13 shows the result of a computer simulation for a 5-min diffusion at 725 °C, including the concentrations of Zn_s^-, $Zn_i^{+\,+}$, and Zn_i^+. Figure 14 shows SIMS data for a 5-min diffusion at 725 °C along with a computer calculated profile.

This model has been used to fit our experimental data over a temperature range from 650 to 750 °C, with results similar to Fig. 14. For any given temperature, this model predicts a constant profile shape which progresses into the GaAs as $t^{1/2}$, in accordance with our data. Table I lists the model parameters used to fit each temperature. $D_{\parallel}$ and D_i do not show any definite trend with temperature, reflecting the data of Fig. 2. This observation has been made before with Zn diffusions under other conditions,[10,11] and is often associated with an interstitial diffusion mechanism. Note that $D_{\parallel}$ and D_i are *effective* diffusivities, meaning that they depend on both the interstitial diffusion rate and the interstitial concentration. The erratic behavior of $D_{\parallel}$ and D_i with temperature is probably due to a decrease in interstitial concentration with temperature (since Zn surface concentration falls as temperature rises) and an increase in interstitial diffusivity. The value of parameter k_2 is consistent with assuming that $Zn_i^{+\,+}$ is a deep donor roughly 0.2 eV from the valence edge, the exact donor level varying with temperature. Since our model has four parameters which affect profile shape, fitting the data with these four parameters is not by itself an adequate test of the model. A good test would be an independent determination of the effective diffusion coefficients $D_{\parallel}$ and D_i, especially their variation with temperature. More experiments involving the variation of the profile shape with time would also be valuable.

V. SUMMARY AND CONCLUSIONS

We have studied the diffusion of Zn into GaAs using diethylzinc and trimethylarsenic sources. This method yields good control over Zn surface concentration and junction depth. The variation of the diffusion profile with time, temperature, and alkyl partial pressures has been examined.

These diffusions have a complex double profile which is not predicted by the interstitial-substitutional model for Zn diffusion. We suggest that this double profile may be caused by the existence of two mobile Zn species which dominate in different regions according to the position of the Fermi level. We have implemented a computer simulation which gives an approximate solution based on this two-species model. The simulation gives a good fit to our experimental data.

Zn diffusion in GaAs is a complicated process. Present experimental data do not completely validate our model nor the existing alternatives. The lack of time dependence (of the profile shape) we observe may simply be a special case of Tuck's[5] or Gösele's[9] model for a short diffusion times. Our model shows, however, that a double diffusion profile does not necessarily imply vacancy (or interstital) nonequilibrium.

ACKNOWLEDGMENTS

We would like to acknowledge the support of J. Zavada at the Army Research Office and D. A. Reynolds at the

Defense Advanced Research Projects Agency. S. Reynolds acknowledges the support of an Office of Naval Research Fellowship.

[1]S. Ghandhi, *VLSI Fabrication Principles* (Wiley, New York, 1983).
[2]M. Dohsen, J. Kasahara, Y. Kato, and N. Watanabe, Electron Device Lett. **2**, 157 (1981).
[3]F. Frank and D. Turnbull, Phys. Rev. **104**, 617 (1956).
[4]L. Weisberg and J. Blanc, Phys. Rev. **131**, 1548 (1963).
[5]B. Tuck and M. Kadhim, J. Mater. Sci. **7**, 585 (1972).
[6]B. Tuck and A. Houghton, J. Phys. D **14**, 2147 (1981).
[7]Performed at Charles Evans and Associates, Redwood City, CA.
[8]C. Ting and G. Pearson, J. Electrochem. Soc. **118**, 1454 (1971).
[9]U. Gösele and F. Morehead, J. Appl. Phys. **52**, 4617 (1981).
[10]See, for instance, S. Ghandhi, *VLSI Fabrication Principles* (Wiley, New York, 1983), p. 654.
[11]C. Ting, Ph.D. dissertation (Standford University, 1968).
[12]M. Kadhim and B. Tuck, J. Mater. Sci. **7**, 68 (1972).
[13]A. Wang, Ph.D. dissertation (Stanford University, 1970).
[14]W. A. Harrison, Phys. Rev. B **31**, 2121 (1985).

Part 4

List of Scientific Personnel

1. James F. Gibbons, Principal Investigator
2. Graduate Students:
   (a) Mark E. Greiner*
   (b) Judy L. Hoyt*
   (c) Walter G. Opyd
   (d) Scott K. Reynolds*
   (e) Dietrick W. Vook

* indicates Ph.D. earned while employed on this project